Using ephaptic coupling to estimate the synaptic cleft resistivity of the calyx of Held synapse.

Short title: **Electronic model of the synaptic cleft.**

Martijn C. Sierksma & J. Gerard G. Borst

Department of Neuroscience, Erasmus MC, University Medical Center Rotterdam, 3000 CA, Rotterdam, The Netherlands.

Correspondence to g.borst@erasmusmc.nl

A conference paper including parts of this paper was presented at Proceedings of the 23rd International Congress on Acoustics (2019, doi: 10.18154/RWTH-CONV-240008)

Keywords: Prespike; Cleft conductance; Giant synapse; Cleft potential; Auditory brainstem; phasor.

Abstract

At synapses, the pre- and postsynaptic cell get so close that currents entering the cleft do not flow exclusively along its conductance, g_{cl}. A prominent example is found in the calyx of Held synapse in the medial nucleus of the trapezoid body, where the presynaptic action potential can be recorded in the postsynaptic cell in the form of a prespike. Here, we developed a theoretical framework for ephaptic coupling via the synaptic cleft. We found that the capacitive component of the prespike recorded in voltage clamp is closely approximated by the second time derivative of the presynaptic action potential. Its size scales with the fourth power of the radius of the synapse, explaining why intracellularly recorded prespikes are uncommon in the CNS. We show that presynaptic calcium currents can contribute to the prespike and that their contribution is closely approximated by the scaled first derivative of these currents. We confirmed these predictions in juvenile rat brainstem slices, and used the presynaptic calcium currents to obtain an estimate for g_{cl} of ~1 μS. We demonstrate that for a typical synapse geometry, g_{cl} is scale-invariant and only defined by extracellular resistivity, which was ~75 Ωcm, and by cleft height. During development the calyx of Held develops fenestrations. These fenestrations effectively minimize the cleft potentials generated by the adult action potential, which would otherwise interfere with calcium channel opening. We thus provide a quantitative account of the dissipation of currents by the synaptic cleft, which can be readily extrapolated to conventional, bouton-like synapses.

Author Summary

At chemical synapses two neurons are separated by a cleft, which is very narrow. As a result, the concentration of released neurotransmitter can rapidly peak, which is essential for fast synaptic transmission. At the same time, the currents that flow across the membranes that face the synaptic cleft are also substantial, and a fraction of these currents will enter the other cell. We made an electronic model of the synaptic cleft, which indicated that if the size of the membrane currents that flow across both membranes are known, our model can be used to infer the electrical resistance of the synaptic cleft. We tested several of the predictions of our model by comparing the membrane currents during a presynaptic action potential in a giant terminal, the calyx of Held, with the much smaller prespike evoked by these currents in the postsynaptic cell. We estimate the cleft resistance to be about 1 MΩ, which means that the changes in the cleft potential due to the membrane currents can become large enough to have an impact on voltage-dependent calcium channels controlling neurotransmitter release.

Introduction

When sir Sherrington introduced the term ‘synapsis’ [1], it was still unknown whether or not nerve impulses reach their target through direct electrical coupling [2, 3]. Together with other evidence, it was the visualization by electron microscopy of the synaptic cleft, the narrow gap between an axon and its target, which put the debate to rest in favor of transmitter-mediated neurotransmission [4-6]. At about the same time, Eccles and Jaeger (7) outlined the electrical circuitry of the synapse, which included a cleft leak conductance (g_{cl}) linking synaptic currents with the interstitial space. Since then, the role of the synaptic cleft for synaptic transmission has gradually become more important. Its small volume not only allows a rapid buildup of released neurotransmitter, but protons [8, 9], and potassium ions [10-12] may accumulate as well, whereas calcium ions may become partially depleted [13, 14]. Interestingly, during transmission a cleft potential may arise that may alter the dwelling time of mobile, charged particles within the cleft [15, 16], the distribution of ligand-gated ion channels [17], or the kinetics of voltage-gated channels in the cleft-facing membrane [18]. These features all stem from the small size of the synaptic cleft, which thus forms a barrier for particle movements [19].

Except for some specialized synapses, the contribution of g_{cl} to synaptic transmission has largely been ignored or deemed irrelevant, but its importance will of course depend on its magnitude and on the size of the currents that flow within the cleft. Eccles and Jaeger (7) already indicated that the maximal cleft current will be limited by this conductance. g_{cl} decreases as the path length l_{path} to the extracellular space increases ($g_{cl} \sim A/(R_{ex}\, l_{path})$, where R_{ex} is extracellular resistivity in Ω cm and A the area through which the current flows (see also Savtchenko, Antropov (20)). Due to their much longer path length, it has been argued that giant synapses have a lower g_{cl} than conventional synapses [21]. Remarkably, estimates of g_{cl} of very different synapses vary over four orders of magnitude (range 1.4 nS to 40 μS) without a clear relation to synapse size [7, 11, 18, 20, 22-30]. Despite the remarkable progress in our understanding of the synaptic cleft, we need a better theoretical understanding of its conductive properties, which is ideally confirmed by experimental observations.

One of the largest synapses in the mammalian brain is the calyx of Held synapse, which spans about 25 µm [31, 32]. Its large size matches its strength, with the maximal glutamatergic conductance exceeding 100 nS, and its fast presynaptic AP allowing firing rates >300 Hz [33]. Large currents, related to the excitatory postsynaptic current (EPSC) and capacitive currents, need to flow within the cleft through g_{cl}, and under these conditions g_{cl} may limit synaptic transmission. A characteristic feature of this synapse is that the presynaptic AP can be detected in the postsynaptic recording (Figure 1). This hallmark of the calyx of Held synapse has been called the prespike [34]. It is probably due to ephaptic coupling of the presynaptic AP via the synaptic cleft [30, 35], but the precise relation between the presynaptic AP and the prespike has not been studied. Here, we use the prespike to infer some key electrical properties of this giant synapse. We provide a theoretical description of ephaptic coupling by defining the electrical properties of the synaptic cleft, which is validated through dual patch-clamp recordings of the calyx of Held and its postsynaptic target.

Results

The prespike is the ephaptically coupled calyx of Held AP recorded in its target neuron, a principal neuron in the medial nucleus of the trapezoid body (MNTB) [34]. Some current clamp (CC) and voltage clamp (VC) prespike examples are shown in Figure 1A-B. Figure 1C shows that the amplitudes of the CC and the VC prespikes recorded in the same cell are correlated. Figure 1D shows examples of the CC prespikes recorded during *in vivo* whole-cell recordings in young rats, whose shape resemble those recorded in the simultaneous pre- and postsynaptic slice recordings (Figure 1A-B, 2A).

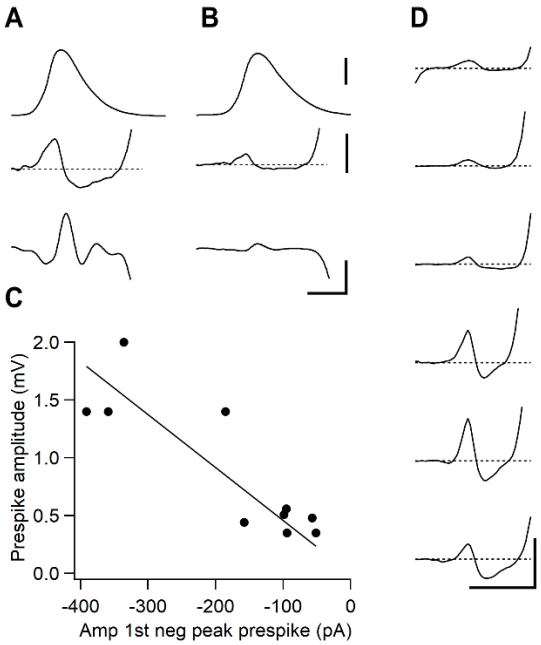

Figure 1 – Examples of prespikes. (A-B) Two examples of prespikes in simultaneous pre- and postsynaptic patch-clamp recordings. From top to bottom: calyx of Held AP, which was elicited by afferent stimulation, CC prespike, associated VC prespike. Recordings were made at room temperature in brainstem slices from 7-10 days old Wistar rats [36]. Horizontal scale bar: 0.5 ms. Vertical (from top to bottom): 50 mV, 2 mV, 1 nA. (C) Relation between amplitude of the positive peak of the prespike measured in CC and the amplitude of the first negative peak of the prespike measured in VC in the same cell. Slope of the fitted line is -4.6 mV/nA. (D). Six examples of CC prespikes from *in vivo* recordings of a target neuron of the calyx of Held in 3-5 days old Wistar rats [37]. During this period the calyx of Held expands over the postsynaptic cell. Note the small upward

deflection immediately preceding the EPSP in the bottom three prespikes. Scale bar indicates 0.5 mV and 0.5 ms.

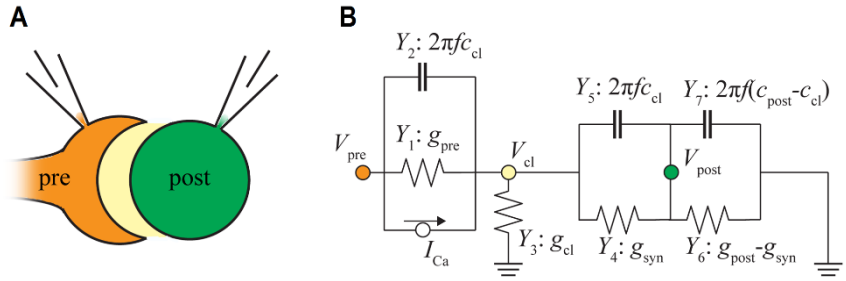

Figure 2. An electrical circuit for the prespike. (A) Drawing of the calyx of Held synapse. The calyx of Held terminal ('pre') covers a large part of the soma of its target neuron ('post'). In between is the synaptic cleft (not drawn to scale), a small space where membrane currents will flow during a presynaptic AP. (B) Electrical circuit to reproduce the prespike. The capacitance facing the cleft (c_{cl}) is assumed to be equal for the calyx and its target. Presynaptic membrane currents can leave the synaptic cleft via the cleft conductance (g_{cl}) or through the postsynaptic cell. It is assumed that the conductance from cleft to ground is relatively large compared to the cleft conductance [38, 39].

Phasor analysis of an electrical circuit for the prespike

The prespike is generated by currents that flow from the calyx to the principal neuron in the MNTB. While the current flow through the cleft depends on the synapse geometry, which we will consider later in this article, we can already get a good understanding by analyzing a prespike-generating, electrical circuit [30] with the following components (Figure 2B): (1) the terminal's release face, consisting of voltage-gated conductances (not shown), a capacitor (c_{cl}), and a conductance (g_{pre}); (2) the synaptic cleft, which is separated from the reference by a leak conductance (g_{cl}), and (3) a passive neuron, which partly faces the synaptic cleft. This part consists of a capacitor (c_{cl}) and a leak conductance (g_{syn}). The remainder of the postsynaptic cell consists of a capacitor (c_{post}-c_{cl}) and a leak conductance (g_{post}-g_{syn}). As the prespike is small, we ignore the

postsynaptic voltage-dependent conductances. We also did not include a direct resistive connection between calyx and target since there is no physiological evidence for gap junctions at the calyx of Held synapse [40], and capacitive currents are likely to dominate the electrical coupling: the susceptance at 1 kHz across an area of 1000 μm^2 is 63 nS ($2\pi f C_m A$, where f is the frequency component, C_m is the specific capacitance, and A the membrane area), which is much larger than the postsynaptic resting conductance of ~4 nS.

We use phasors to describe analytically how currents flow and voltages change within this circuit in response to the presynaptic AP. In our notation, capitals indicate phasors, e.g. V, I; lowercases indicate real-valued responses, v, i; j indicates the imaginary number $\sqrt{-1}$. To come to an analytical description of the prespike, we first describe the relation between the presynaptic AP and the cleft potential. The cleft potential can be approximated as the presynaptic potential multiplied by the voltage divider formed by the presynaptic capacitance Y_2 and the parallel combination of cleft conductance Y_3 and postsynaptic capacitance: $V_{cl} = V_{pre}(-jY_2)\left(Y_3 - j(Y_2 + Y_5)\right)^{-1}$ (Appendix A1.1). This notation can be transformed to an angular notation, which shows how amplitudes are scaled by the modulus and shifted in time by the phase shift: $V_{cl} = V_{pre}\, 2\pi f \tau_{cl}\, ((4\pi f \tau_{cl})^2 + 1)^{-0.5} \angle\, atan2(-1, 4\pi f \tau_{cl})$ (Appendix A1.2 and A1.3), where the cleft time constant τ_{cl} is defined as $\tau_{cl} = c_{cl}/g_{cl}$. These phasor relations can be simplified when we assume that g_{cl} is substantially higher than the cleft susceptance ($g_{cl} >> 2\pi f c_{cl}$). The cleft potential then becomes $V_{cl} = V_{pre} 2\pi f \tau_{cl} \angle\, atan2(-1, 4\pi f \tau_{cl})$ (Appendix A1.6). We thus observe a prominent contribution of the frequency component (f), indicating that faster voltage and current changes will be more readily transmitted. We see that v_{cl} is a high-pass filtered v_{pre}, and that it approaches the first derivative of v_{pre} (as the phase shift approaches $-\pi/2$). This is to be expected as the current that enters the synaptic cleft is mainly the capacitive current $c_{cl}\, dv_{pre}/dt$. Using the waveform of a presynaptic AP, we can calculate the cleft potential (Figure 3A-B), which, indeed, resembles the biphasic capacitive current.

These changes in v_{cl} will generate a postsynaptic current, the VC prespike, $I_{post} = -jY_5V_{cl}$, which yields $I_{post} = -V_{pre}\, g_{cl}(2\pi f\tau_{cl})^2((4\pi f\tau_{cl})^2 + 1)^{-0.5}\, \angle atan2(-4\pi f\tau_{cl},\ -1)$ (Appendix A2.1-2.5; we use the convention that an inward current is negative). This current underlies the CC prespike, which can be described as $V_{post} = -I_{post}\,(Y_4 - jY_5 + Y_6 - jY_7)^{-1}$, which gives $V_{post} =$

$$V_{pre}(2\pi f c_{cl})^2\ \left(\left[{g_{post}}^2 + \left(2\pi f c_{post}\right)^2\right]\left[{g_{cl}}^2 + (4\pi f c_{cl})^2\right]\right)^{-0.5}$$

$\angle atan2\left(-\left(2\pi f c_{post} g_{cl} + 4\pi f c_{cl} g_{post}\right), -g_{post} g_{cl} + (2\pi f)^2 c_{post} c_{cl}\right)$ (Appendix A3.1-3.7). When we again assume that g_{cl} is substantially higher than the cleft susceptance, the VC prespike becomes $I_{post} = -V_{pre}\,(2\pi f\tau_{cl})^2 g_{cl}\, \angle atan2(-4\pi f\tau_{cl}, -1)$ (Appendix A2.6); and when we also assume for the CC prespike that the postsynaptic susceptance is substantially higher than the postsynaptic conductance ($2\pi f c_{post} >> g_{post}$), we obtain $V_{post} = V_{pre}\, 2\pi f\tau_{cl}\ \ c_{cl} c_{post}^{-1}$ $\angle atan2\left(-2\pi f\tau_{post}, ((2\pi f)^2\tau_{cl}\tau_{post} - 1)\right)$ (Appendix A3.8 and A3.9). The VC prespike therefore reflects the second derivative of v_{pre} scaled by g_{cl} as the phase shift approaches $-\pi$ (Figure 3C).

Lastly, the CC prespike is the first derivative of v_{pre} scaled by the relative postsynaptic cleft capacitance (Figure 3D).

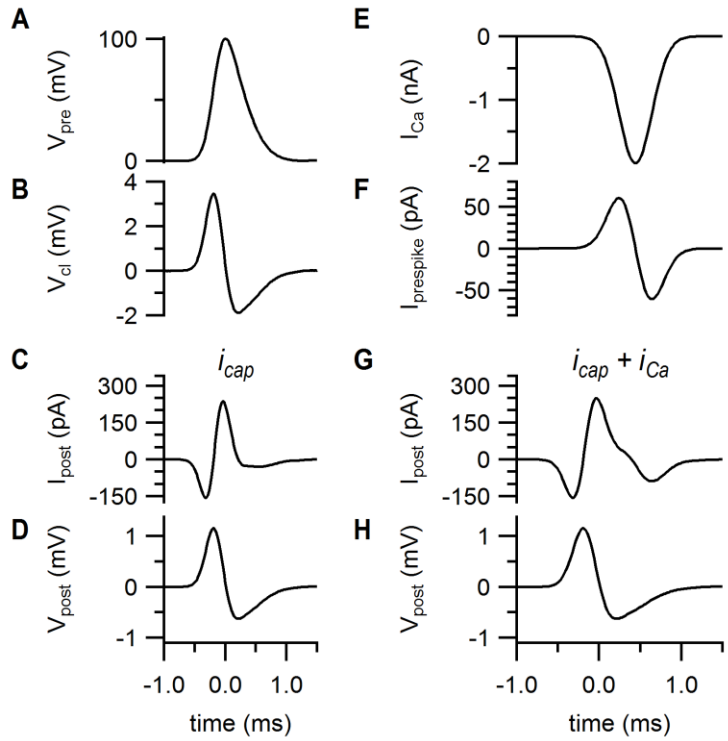

Figure 3 – Transformation of the presynaptic AP by phasors yields prespike-like responses. (A) An AP waveform used in voltage-clamp experiments to elicit presynaptic calcium currents. (B-D) The capacitive response in the cleft potential (B), in the capacitive prespike currents (C), and in the capacitive prespike potentials in response to the presynaptic AP (D). (E) The calcium current can be simulated as a Gaussian function. (F) The calcium prespike in response to the calcium current. (G-H) The VC prespike (G) and CC prespike (H) in response to both the capacitive current and the calcium current. G is the combined currents in C and F. The parameter values were: c_{cl} = 10 pF, g_{cl} = 1 μS, c_{post} = 30 pF, g_{post} = 5 nS, q_{ca} = 1 pC, and τ_{Ca} = 0.21 ms. The calcium current peak was aligned with a membrane potential of +30 mV relative to the resting potential on the downward slope of the AP waveform.

It is more challenging to obtain an analytical description for the impact of the voltage-gated conductances on the prespike, as these conductances depend on the transmembrane potential at the cleft-facing membrane, and therefore are not expected to remain constant in time. However, if the amplitude and time course of an ionic current (i_{ion}) are known, its impact on the prespike currents

171 can be described as $I_{post} = I_{ion}\,(-jY_5)(Y_3 - j(Y_2 + Y_5))^{-1}$, which simplifies to $I_{post} =$

172 $I_{ion} 2\pi f \tau_{cl} \angle\, atan2(-1, 4\pi f \tau_{cl})$ (Appendix A4.1). The calcium current of the calyx of Held closely

173 follows a Gaussian function [41], which has the advantage that its Fourier transform is another

174 Gaussian function. We describe the calcium current with a charge transfer q_{ca} centered at its peak

175 as $i_{ca} = i_{peak}\exp(-0.5(t/\tau_{Ca})^2)$ (Appendix 4.2; Figure 3E; τ_{Ca} corresponds to the standard

176 deviation of the Gaussian function). Its Fourier transform is $I_{ca} = q_{ca}\exp(-2(\pi\tau_{Ca} f)^2)$ (Appendix

177 4.3). We multiply I_{ca} with the transfer function and perform an inverse Fourier transform: $i_{post}(t) =$

178 $-\tau_{cl}\, i_{peak}\tau_{Ca}^{-2}\, t\, \exp(-0.5(t/\tau_{Ca})^2)$, which is $-\tau_{cl}\, \mathrm{d}i_{Ca}/\mathrm{d}t$ (Appendix A4.4-A4.6). This shows a

179 biphasic response with a positive and a negative peak (Figure 2F) at $\pm\, \tau_{Ca}$ with an amplitude of

180 $\tau_{cl}(\tau_{Ca}\sqrt{e})^{-1}\, i_{peak}$. We therefore define a simple scaling factor $\tau_{cl}/(\tau_{Ca}\sqrt{e})$ that (with a phase shift)

181 relates the presynaptic calcium current amplitude to a biphasic, postsynaptic current. This biphasic

182 response is only the calcium component of the VC prespike (the calcium prespike), and it needs to

183 be combined with the capacitive currents generated by the presynaptic AP (the capacitive prespike)

184 to obtain the VC prespike (Figure 3G) and subsequently the CC prespike (Figure 3H). We observe

185 that the first part of the VC prespike, including its first negative peak, is mainly due to the

186 capacitive prespike, while the last part with the second negative peak is mostly due to the calcium

187 prespike.

188

189 **Experimental validation of the model**

190 Based on our phasor analysis, we predict that the VC prespike resembles the second derivative of

191 the presynaptic AP. To test this prediction, we revisited published simultaneous whole-cell

192 presynaptic current clamp recordings with postsynaptic voltage clamp recordings [36, 42]. In these

193 recordings, the afferent axon of the calyx of Held was stimulated with an electrode to trigger a

194 presynaptic AP, and a prespike followed by an EPSC was recorded postsynaptically (Figure 4A).

195 The prespike generally matched the scaled inverted second derivative of the AP (Figure 4A-B),
196 taking into account that it may have been filtered by the series resistance. Figure 4B shows that in
197 these recordings the time course of the second derivative of the AP indeed provides a better match
198 for the prespike than its first derivative (n = 13 paired recordings). This is in agreement with the
199 idea that the prespike is generated by two capacitors in-series.

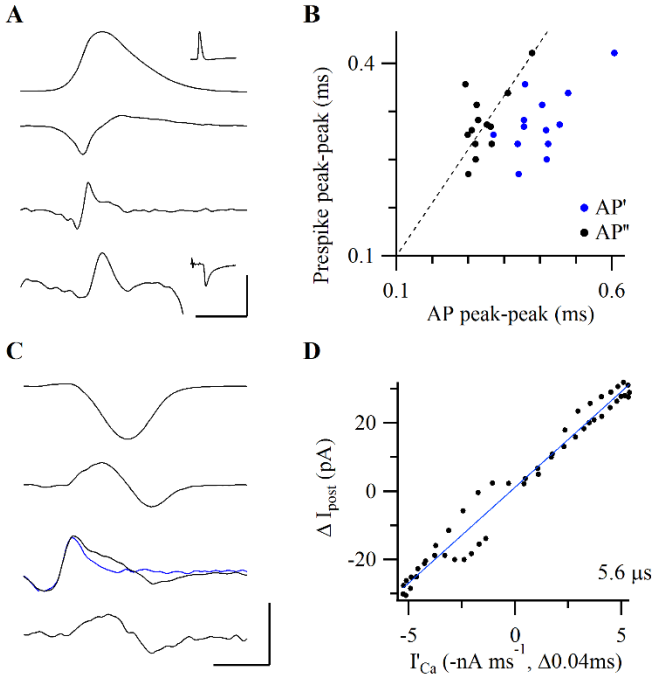

200 **Figure 4 – Relation between the calyceal AP and the prespike.** (A) *Left column, from top to bottom*: AP
201 recorded in CC from the calyx of Held, its inverted first and second derivatives, and postsynaptic voltage clamp
202 recording showing the accompanying prespike. Insets show the same presynaptic AP (top) and the postsynaptic
203 EPSC (bottom) elicited by the calyceal stimulation on a longer time scale. Vertical scale bars (from top to
204 bottom panels): 80 mV, 0.8 kV/s, 8 MV/s^2, 0.2 nA. Horizontal: 0.5 ms. (B) Relation between the delay between
205 the first negative and positive peak of the prespike and the first two peaks in the first (blue) and second (black)
206 derivative of the presynaptic AP. Dashed line is the identity line. (C) *Left column, from top to bottom*:
207 Presynaptic calcium current (after P/5 subtraction), its first derivative, postsynaptic currents (black, active) and
208 passive prespike (blue, P/5-scaled), difference between active and passive prespike (black minus blue), which
209 corresponds to the calcium prespike. Vertical scale bars: 2 nA, 15 nA/ms, 0.15 nA, 0.1 nA. Horizontal: 0.5 ms.
210 (D) Relation between the first derivative of the presynaptic calcium current shown in the bottom panel of C and

211 the calcium prespike. Maximum correlation was obtained when delaying the first derivative by 40 µs. Blue line
212 shows regression line with a slope of 5.6 µs.

213

214 A second prediction of our phasor analysis is that presynaptic calcium currents that arise from the
215 cleft will have an impact on the shape of the prespike. We turned to simultaneous whole-cell pre-
216 and postsynaptic voltage clamp recordings of the calyx of Held synapse that were originally
217 reported in Borst and Sakmann (43), which were re-analyzed to evaluate the presence or absence of
218 a calcium prespike. In these experiments the presynaptic compartment was voltage clamped with an
219 action potential waveform (APW) command while the presynaptic calcium currents were
220 pharmacologically isolated (Figure 4C). To isolate the postsynaptic current related to the calcium
221 currents, we averaged the postsynaptic responses to the P/5 AP waveform and subtracted the scaled
222 passive prespike from the 'active' prespike to obtain the calcium prespike. The remaining currents
223 indeed showed the biphasic response predicted by the phasor analysis (Appendix A4; cf. second and
224 bottom panel of Figure 4C).

225 From the phasor analysis we know that when the presynaptic calcium current and the VC prespike
226 are simultaneously recorded, τ_{cl} can be calculated by comparing di_{Ca}/dt and the calcium prespike.
227 To estimate τ_{cl}, we first analyzed the presynaptic calcium current that was evoked by the APW. It
228 had a peak amplitude of -1.9 ± 0.6 nA and a full-width at half-maximum (FWHM) of 0.51 ± 0.05
229 ms (n = 5 paired recordings). Next, we obtained the values for the calcium prespike. Its peak-to-
230 peak amplitude was 80 ± 60 pA and its peak-to-peak delay was 0.54 ± 0.11 ms. This peak-to-peak
231 delay should be about twice τ_{Ca}, which was thus slightly higher than the 0.21 ms reported by Borst
232 and Sakmann (44). Its time course closely matched the model predictions (*cf.* Figure 4C and Figure
233 3F). As predicted by the phasor analysis, the amplitude of the calcium current was linearly related
234 to the calcium prespike peak (r = 0.98, p = 0.003); the calcium prespike peak was 1.9 ± 0.7% of the
235 calcium current amplitude. Above, we derived that this percentage should be $\tau_{cl}\ \tau_{Ca}^{-1}e^{-0.5}$, yielding

236 an estimated τ_{cl} of 9 ± 5 µs. As an alternative approach, we plot the first derivative of the
237 presynaptic calcium current against the calcium prespike. Its maximal slope (allowing for a slight
238 time shift) provided a τ_{cl} of 6 ± 2 µs (Figure 4D). The two methods thus gave comparable values for
239 the cleft time constant.

240 The ratio of cleft capacitance c_{cl} and cleft leak conductance g_{cl} constitutes τ_{cl}. If we assume that c_{cl}
241 is 10 pF, the estimated g_{cl} becomes about 0.5-1 µS. From the phasor analysis we know that the
242 capacitive VC prespike coming from the presynaptic AP and the calcium prespike do not scale the
243 same way to c_{cl} and g_{cl} (*cf.* Appendix A2.1 with A4.1). This difference allows us to further define
244 these two parameters. We define the relation between the postsynaptic calcium component and the
245 presynaptic calcium current as $I_{post}/I_{Ca} = 2\pi f\tau_{cl} = R_{Ca}$. If we substitute $2\pi f\tau_{cl}$ in equation A2.6 with
246 R_{Ca}, the equation for the capacitive prespike becomes $I_{post} = V_{pre}\, R_{Ca}^2\, g_{cl}$, and the Fourier transform
247 will yield the same scaling factor of $(R_{Ca})^2 g_{cl}$. The first peak of the VC prespike had an amplitude
248 of -120 ± 110 pA, which corresponds to the capacitive currents. We can then calculate a g_{cl} of 2.6 ±
249 0.8 µS and a c_{cl} of 24 ± 16 pF. (In this calculation we assume that the time course of the calcium
250 current and the presynaptic AP have a very similar frequency composition.)

251 For τ_{cl} we assumed that the calcium current entirely originated from the membrane facing the cleft.
252 These estimates should be considered as a lower bound as some of the current may not arise from
253 the cleft-facing membrane. Immunolabeling for calcium channels identified a fraction of the N-type
254 and R-type calcium channels to be in the non-cleft-facing membrane [45]. If we assume that only
255 two-third of the calcium current originated from the cleft, our estimate of τ_{cl} increases to 13.5 ± 7.8
256 µs. This estimate could be considered as an upper bound, as less than 50% of the calcium current
257 was mediated by N-type and R-type channels, and the other, P/Q-type, calcium channels were
258 mostly associated with the release face [45]. When we assume that 2/3 of the total presynaptic
259 calcium current originated from the cleft, we calculate a g_{cl} of 1.2 ± 0.4 µS and a c_{cl} of 16 ± 11 pF.
260 With our limited data set we determine that g_{cl} ranges between 1-2 µS.

261

262 **Cleft currents**

263 For the calyx of Held synapse to be strong and fast, it needs to rapidly conduct large currents. We
264 focus on the generation of the prespike, but a similar analysis can be made for the feedback effect
265 of postsynaptic currents on the calyx of Held [30]. The calyceal EPSC is very fast and can easily be
266 10 nA [36, 46-49]. This EPSC should flow not only through the postsynaptic glutamate receptor
267 channels, but also through g_{cl} [7]. For the synapse to be able to conduct an EPSC of 10 nA at a
268 driving force of 100 mV, the cleft leak conductance must be at least >0.1 μS. This is consistent with
269 the observed range for g_{cl}.

270 Besides the capacitive currents and the EPSC, voltage-gated channels facing the cleft may also
271 contribute to the cleft currents. We therefore explored the potential contribution of Na^+ and K^+
272 currents to the prespike. We estimated their density based on literature values, and assumed a
273 homogeneous distribution within the terminal. As voltage-gated channels in the cleft-facing
274 membrane sense v_{pre}-v_{cl} instead of v_{pre}, their gating depends on v_{cl}. This feedback effect of v_{cl} could
275 not be incorporated in the phasor calculations. We instead simulated the consequences of v_{cl} on
276 voltage-gated currents by numerically solving ordinary differential equations with different values
277 for g_{cl}. Figure 5 illustrates that the presence of these channels at the release face may have a large
278 impact on the shape and size of the prespike. Due to the differences in their gating properties, the
279 timing of each current during the presynaptic AP is quite different (Figure 5A), and the same holds
280 for their impact on v_{cl} and on the prespike (Figure 5B). The prespike examples (Figure 1) did not
281 resemble the prespike of the homogeneous model, which included Na^+, K^+ and Ca^{2+} currents at the
282 cleft-facing membrane, suggesting that some voltage-gated ion channels are excluded (at least
283 functionally) from the release face. In particular, the voltage-gated sodium conductance generates a
284 current that partially counteracts the first prespike peak. These very fast changes in the prespike
285 during the rising phase of the presynaptic AP would point at a contribution by sodium channels. As

these were not observed, we conclude that there is no substantial contribution of sodium channels at the release face to the prespike.

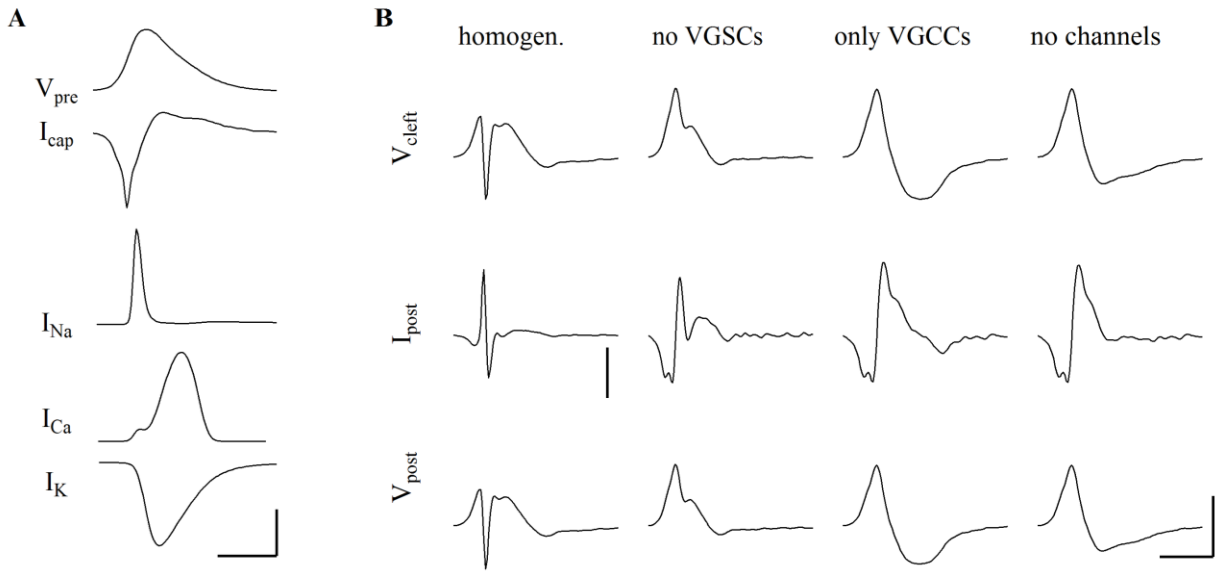

Figure 5 – Impact on the prespike of voltage-gated ion channels located at the release face. (A) Timing of different voltage-gated currents at the release face during the AP. Note that the amplitudes of each of the currents depend on cleft potential, thus creating a mutual dependency. Vertical scale bar: 60 mV, 2.4 nA, 1 nA, 1 nA, 3 nA. Horizontal: 0.5 ms. (B) The cleft potential (top), the VC prespike (middle), and the CC prespike (bottom) under different conductance density conditions. Homogen.: homogeneous density; no VGSCs: no sodium conductance at the release face; only VGCCs: calcium and capacitive currents at the release face; no channels: the capacitive-only model. Scale bars: 4 mV, 0.2 nA, 2 mV.; 0.5 ms, except for the homogeneous model where the vertical scale bar corresponds to 1.6 nA.

Potassium channels do not start to open until around the peak of the presynaptic AP. They therefore do not impact the first part of the VC/CC prespike. The potassium current contributes to a more positive synaptic cleft potential, which would be opposite to the effect of the calcium current. If the potassium current at the cleft were significantly larger than the other currents, we would expect a fast inward current in the VC prespike after the first positive peak, and the CC prespike would become a single positive deflection.

However, CC prespikes are typically biphasic (Figure 1), therefore the contribution of the potassium current is unlikely to outweigh the contribution of the other currents.

Lastly, we revisit the impact of calcium channels on the prespike. The observation of a calcium prespike already demonstrated the presence of these channels at the release face. The calcium current occurs during the repolarization phase of the presynaptic AP [44], and therefore contributes little to the first two peaks of the VC or to the first peak of the CC prespike. Its contribution is easily obscured by noise or by the EPSC, which starts rapidly after the calcium-induced glutamate release. Nevertheless, it may generate a small, upward inflection in the CC prespike and such an inflection can sometimes be observed (Figure 1D).

These simulations show that the prespike waveform may contain information about the presence of voltage-dependent ion channels at the presynaptic membrane facing the cleft. This means that a comprehensive experimental study of the impact of specific channel blockers on the prespike waveforms in experiments similar to Figure 3 may be informative about their presence at the release face.

Voltage-dependent kinetics of cleft-facing calcium channels

During development the presynaptic AP narrows from a half width of 0.5 to 0.2 ms [46]. The briefer AP necessitates a much larger capacitive current, which, all else being equal, would generate a larger change in v_{cl}, which may impact the calcium channel kinetics. We again simulated the impact of v_{cl} on the calcium current by solving ordinary differential equations for different values for g_{cl} (Figure 6). For a slow AP, a g_{cl} of 0.67 µS and a c_{cl} of 10 pF, v_{cl} first rises to a maximum of +3.9 mV, and then decreases to a minimum of -4.2 mV. While v_{cl} has little effect on the current amplitude (Figure 6B), it generates a delay of 45 µs in the onset of the calcium current (Figure 6C). In contrast, under the same conditions we observe for a fast AP that v_{cl} rises to a maximum of +16.4 mV, followed by a decrease to a minimum of -8.2 mV. As a consequence, the peak calcium current

was delayed by 21 µs and reduced by 19% (-2.0 nA vs -1.7 nA). These effects became even more pronounced at lower g_{cl}. The observed delay corresponded to the delay in reaching the $v_{pre} - v_{cleft}$ maximum compared to the v_{pre} maximum; the reduction in calcium current was due to a smaller effective AP, which reduced the maximal open probability of the calcium channels. We conclude that developmental acceleration of the calyceal AP will increase the capacitive current to a level that potentially could delay and impede the presynaptic calcium current substantially if g_{cl} were <1 µS.

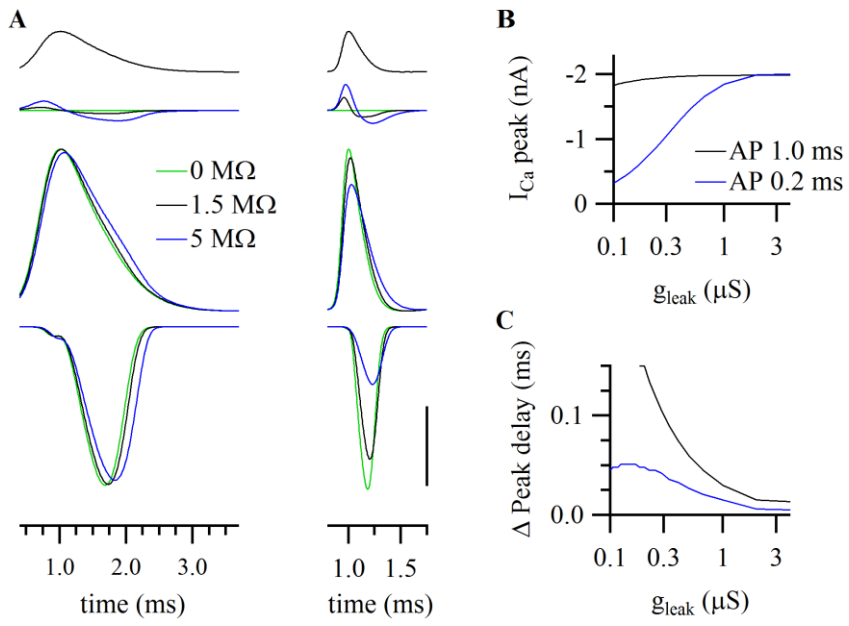

Figure 6 – Potential impact of the cleft potential on presynaptic calcium currents. (A) Simulation of the impact of a slow and a fast AP (top; FWHM: left 1.0, right 0.2 ms) on the cleft potential (second row), the transmembrane potential sensed by the calcium channels in the cleft (third row) and the presynaptic calcium current (bottom) at three leak resistances (0 MΩ, 1 MΩ and 5 MΩ). Scale bar: 228 mV, 103 mV, 57 mV, 1 nA. (B) Relation between peak calcium currents and leak resistance for the two APs. Driving force slightly increases (not shown). (C) The change in delay between the calcium peak current and the AP for the two APs (solid line). The dashed line shows the delay after correcting for the decrease in the calcium current shown in B. Calcium conductance density was adjusted to 0.2 nS μm^{-2} and 2.8 nS μm^{-2} for the slow and fast AP, respectively, in order to elicit a 2 nA-current at 0 MΩ cleft leak resistance. The apposition area was 1000 μm^2.

Other conductances were set to 0 nS.

Fenestration of the calyx of Held reduces cleft potentials.

So far we modeled the cleft as a single compartment with capacitive and conductive properties. However, it is expected that the voltage profile within the cleft will depend on synapse geometry [20]. We therefore need an analytical description of the voltage profile within the cleft. Previous work considered the impact of cleft geometry on the EPSC, a current that runs radially through the cleft and enters at a centered region containing the glutamate receptors [20]. Our situation is different as we consider a homogeneously distributed current: the capacitive currents arise at every membrane patch facing the cleft. For an analytical description we start by assuming a radially-symmetric synapse with a radius r and a cleft height h. Within this synapse we only consider capacitive currents from the cleft-facing membrane (Figure 7A). As only a small fraction of these currents enters the postsynaptic cell, we simply assume that all currents run radially to the synaptic membranes. The electric field at location x relative to the cleft center will be $dv_{cl}/dx = xR_{ex}C_m(2h)^{-1}dv_{pre}/dt$ (Appendix B1.3) where R_{ex} is the extracellular cleft resistivity and C_m is the specific membrane capacitance. The electric field grows linearly with the distance from the center. The cleft potential is equal to $\int_x^r dv_{cl}\,dx$, which gives $v_{cl} = (r^2 - x^2)R_{ex}C_m(4h)^{-1}dv_{pre}/dt$ (Appendix B1.4). The size of the cleft potential thus depends on r^2, indicating that for larger terminals the cleft potential may become increasingly important (Figure 7B). The voltage profile also shows that not all voltage-gated channels in the cleft will be affected, but only the channels located towards the cleft center.

The temporal changes in the cleft potential will generate a capacitive current at the postsynaptic side. To obtain the VC prespike, we derive $i_{post} = r^4\pi R_{ex}C_m^2(8h)^{-1}d^2v_{pre}/dt^2$ (Appendix B2.2). The VC prespike therefore grows with the fourth power of the radius, which explains why prespikes are only observed in giant synapses such as the calyx of Held synapse. With our geometrical relation for the VC prespike we can relate g_{cl} to extracellular resistivity: $g_{cl} = 8\pi h(R_{ex})^{-1}$ (Appendix B3). This relation

leads to an estimate for the intra-cleft resistivity of 75 Ω cm for an h of 30 nm [50] and a g_{cl} of 1 μS. Considering that there may be extended extracellular spaces within the synaptic cleft [51], and taking into account the variation in g_{cl} (1-2 μS), we estimate an R_{ex} in the range of 50-100 Ω cm.

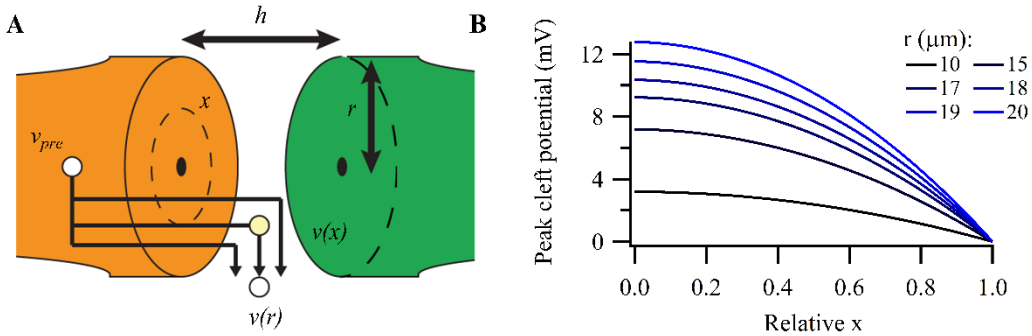

Figure 7. Synapse geometry determines the profile of the cleft potential. (A) Drawing of a radially-symmetric synapse with cleft height h and radius r. The capacitive currents will generate a cleft potential v(x) at location x. (B) Cleft voltage profile for synapses with different radii (color-coded) at the first peak in the capacitive current. The horizontal axis depicts the location from the center (0) relative to the edge (1.0). In (B), R_{ex} is 100 Ω cm, C_m is 1 μF cm^{-2}, and h is 30 nm.

Giant synapses typically fenestrate during development [52-55]. We initially assumed that fenestration minimizes v_{cl} by reducing g_{cl} through reducing the path length to the extracellular fluid (r). However, we analytically derived that for a radially-symmetric synapse, g_{cl} does not dependent on its radius. The relation between the conductance and the resistivity is $g_{cl} \sim A\ (r\ R_{ex})^{-1}$, where A is the area through which the current escapes. As A of a radially-symmetric cleft is $2\pi rh$, when r is doubled, A is also doubled, leaving the conductance independent of synapse size. The cup-shape of the young calyx makes the radially-symmetric synapse a reasonable approximation. This also means that our estimate of the resistivity of the synaptic cleft is relevant for smaller synapses with a comparable radially-symmetric shape.

Following a period of fenestration, the calyx of Held becomes, as its name implies, a synapse with extended fingers [31, 56]. However, for finger-like synapses with a sheet-like or cylindrical cleft, the geometrical relations are slightly different. For these synapses we assume that the currents only run transversally, *i.e.* perpendicular to the longitudinal axis. The cleft potential then becomes $v(x) =$

$(r^2 - x^2)(2h)^{-1}R_{ex}C_m dv_{pre}/dt$ (Appendix B4.4), where 2*r* equals the width of the sheet (or *r* the length of the cylinder). As the escape route for the current is more restricted than for a radially-symmetric synapse, its voltage gradient is steeper. However, the diameter of a calyceal finger will be much less than the diameter of the juvenile calyx, effectively reducing the cleft potential. For a calyceal finger of 4 µm diameter [31, 57] the cleft potential at the center of the finger-like synapse would be only ~2.5% of the cleft potential in the cup-shape calyceal synapse (equation B5.2). As a consequence, the VC prespike would become ~3.3% assuming that the total contact surface is conserved (equation B5.4). The cleft potential and VC prespike with more complex synapse morphology may be investigated using finite-element modeling, but this is beyond the scope of this study.

Fenestration will effectively reduce the amplitude of the cleft potentials, and therefore we expect that the prespike in the adult calyx of Held synapse should be significantly smaller than the juvenile prespike. To study the adult prespike, we revisited *in vivo* whole-cell current-clamp recordings of MNTB principal neurons from wild-type C57BL/6J mice previously reported in Wang, van Woerden (58) or in Lorteije, Rusu (59). CC prespikes consisted of a small positive deflection, preceding the start of the rapid rising phase of the EPSP by about 0.3 ms. In 11 of 12 recordings, the amplitude of the positive deflection was <0.2 mV. In contrast to the juvenile recordings (Figure 1), the positive peak was not followed by a negative peak. An example is shown in Figure 8. The good correlation between the size of CC and VC prespikes (Figure 1C) in combination with the absence of a large decrease in the input resistance of adult principal neurons [58, 59] suggests that the VC prespike can be expected to also be relatively small. Our anecdotal evidence from *in vivo* whole-cell recordings in adult mice therefore confirms that the prespike is smaller than the juvenile prespike and that it possibly has a different shape (*cf.* Figure 1 and 8).

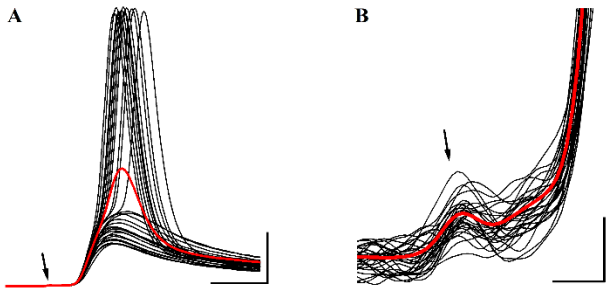

Figure 8 – Adult prespike. (A) Black traces: Spontaneous, sub- and suprathreshold events recorded during a whole-cell *in vivo* recording of a principal neuron in the MNTB from a P52 C57BL/6J mouse [58]. Events were aligned on the start of their EPSP and (<1 mV) differences in the resting membrane potential between events were subtracted for the display. Minimum interval between events was 20 ms. Red trace: average of >1000 events. Resting potential was -64 mV. Arrow points at the small prespike. Vertical scale bar: 10 mV. Horizontal: 1 ms. (B) As (A), showing closeup of the prespike (arrow). Vertical scale bar: 0.2 mV. Horizontal: 0.2 ms.

Discussion

Here, we studied how electrical currents that are needed to depolarize a presynaptic terminal or trigger transmitter release are dissipated in the synaptic cleft. We derived equations for the ephaptic coupling between the presynaptic terminal and the postsynaptic cell. We found that the capacitive component of the prespike is closely approximated by the second time derivative of the presynaptic action potential. Its size scales with the fourth power of the radius of the synapse, explaining why intracellularly recorded prespikes are uncommon in the CNS. We showed that presynaptic calcium currents can contribute to the prespike and that their contribution is closely approximated by the scaled first derivative of these currents. We used their contribution to infer an estimate of the cleft conductance, which was ~1 μS for the juvenile calyx of Held synapse. We showed that the cleft conductance of a radially-symmetric synapse does not depend on its radius, but is entirely defined by its height and the extracellular resistivity. This led to an estimate of the cleft resistivity that is at most 50% larger than of the interstitial fluid, which means that the cleft conductance is large enough to allow for the large EPSCs of the calyx of Held, but small enough to have a potential impact on the opening of presynaptic voltage-dependent calcium channels. Finally, we showed that developmental fenestration of the calyx of Held constitutes a very effective adaptation to minimize synaptic cleft potentials.

Comparison of cleft electrical properties across synapses

Using the calcium component of the prespike, we estimated a cleft conductance of about 1 μS. This value is subject to some uncertainty. For the calculation we assumed that most, but not all, presynaptic calcium channels are facing the synaptic cleft. The juvenile calyx contains N- and R-channels, which are not located near the release sites based on immunostaining and their lower efficacy at triggering release, which is in contrast to the P/Q-type calcium channels [45]. Our assumption that only two-third of the

calcium current originated from the cleft is therefore reasonable, considering that the N- and R-channels make up about half of the calcium currents of the juvenile calyx.

Even though we calculated the AP-related capacitive currents that run through the cleft-facing membrane, we did not record the AP itself at the cleft-facing membrane. The AP passively invades the terminal [60], and therefore may be slowed down and have a reduced amplitude at the cleft-facing membrane. We consider it unlikely that this filtering is significant for two reasons. First, passive filtering from one end to the other end of the calyx reduces the AP peak by only 6 mV with a delay of <0.2 ms [61]. Second, the axonal AP is able to invade the fenestrated endings of the mature calyx [62], which should have a significantly higher impedance than the cup-shaped calyx. Our calculation of the presynaptic capacitive currents as the rate of change of the recorded calyceal AP relative to the cleft potential is therefore likely to be accurate.

Interestingly, with similar values for cleft height and extracellular resistivity other studies came to a wide range of estimated values for the cleft conductance, both at least an order of magnitude smaller than 1 µS [11, 26, 28-30, 63], but in some cases also considerably larger than 1 µS [7, 64]. In some of the synapses, an unusually large and narrow path to the interstitial fluid was responsible for the low estimates. Examples are mossy fiber boutons penetrated by a thin (<1 µm) spinule [28], the unusually long calyx-type vestibular synapse [11], or the cone-to-horizontal cell synapse, for which a large part of the horizontal cell is located within an invagination of the cone photoreceptors [65]. While cleft resistivity should be independent of morphology, the cleft conductance for membrane currents at the deep end of these synapses would be significantly less than for the homogeneously distributed current addressed here. In these morphologically complex synapses, slow removal of ions or neurotransmitter may serve a function, for example in the case of vestibular hair cells, where potassium ions accumulate [10, 11], or in the cone photoreceptor synapse, where prolonged effects of glutamate are important, and where postsynaptic currents are typically relatively small [66]. At the other end of the range lies the high estimate for the cleft conductance of the neuromuscular junction, to which the postjunctional folds were suggested to contribute

[7]. The unique morphological properties of these synapses have therefore made a large contribution to the large range of estimated values for the cleft conductance.

Our calculations indicated that for homogeneously-distributed currents the associated cleft conductance is fully determined by the extracellular resistivity, the cleft height and the morphological type of the synapse, but not by the size of the synapse. The cleft height is constrained within narrow boundaries because of the opposing requirements of low volume for high neurotransmitter concentrations and high conductance to allow large synaptic currents [16]. The cleft height typically ranges across synapses between 10-30 nm, but there is some uncertainty regarding the impact of chemical fixation. Assuming a cleft height of 30 nm, we estimated a resistivity of 75 Ω cm based on the prespike, only about 30% larger than of cerebrospinal fluid or Ringer solution [16, 67]. While we are not aware of other estimates of the extracellular resistivity within the synaptic cleft, our estimate is similar to the intracellular resistivity of neurons [68-70] and the periaxonal resistivity of myelinated axons [70]. The extracellular resistivity can also be estimated based on the diffusional mobility of small molecules. Our estimate agrees with those made with an imaging method in hippocampal mossy fiber synapses, which also estimated that small molecules move on average about 50% slower than in the Ringer solution [71]. Estimates of neurotransmitter diffusion constants within the synaptic cleft range from 1.5 to 4 times smaller than in free solution [72-74], but for neurotransmitters diffusion within the synaptic cleft may be slowed down by neurotransmitter-binding proteins. We therefore suggest that a cleft resistivity of ~75 Ωcm may apply to other synapses as well. Given the range of cleft heights and the estimated cleft resistivity, the cleft conductance can be inferred for a distributed current using our analytical relations (B3.2). It should be not so different from the calyx of Held considering that cleft height is conserved across synapses, while the geometry of the juvenile calyx translates well to bouton synapses by simple downscaling. Cleft conductances for circular synapses would then range between 0.3-1.0 μS.

The prespike: what is it good for?

The extracellular AP of the calyx of Held can be observed in extracellular recordings at the target neuron [75], and the characteristic shape of the complex waveform consisting of the presynaptic AP, the EPSP and the postsynaptic AP has facilitated identification of *in vivo* single unit recordings at the MNTB [59]. Importantly, it was shown that the calyceal AP can be picked up in postsynaptic whole-cell recordings as well [34]. In postsynaptic voltage clamp recordings the prespike showed a resemblance to a high-pass filtered version of the presynaptic AP [36], but we showed here that it is closer to the second derivative of the AP. At the related endbulb of Held synapse, the presynaptic AP is also readily picked up in extracellular recordings [76]. However, no prespikes were reported during postsynaptic whole-cell recordings [77] possibly due to the smaller size of the endbulb compared to the calyx of Held. In the visual system, prespikes can be seen in a subset of lateral geniculate neurons [78]. However, in many synapses in which the presynaptic AP is readily observed in extracellular recordings, it is not reported in intracellular postsynaptic recordings [18, 79-83], attesting to the efficiency of the synaptic cleft in dissipating these currents. Interestingly, especially in the hippocampus, neurons can display so-called spikelets with an amplitude of mV in intracellular recordings. They have a biphasic shape resembling the calyceal prespike recorded in current-clamp. These spikelets are thought to result from ephaptic, capacitive coupling with one or more nearby neurons [84]. The equations we derived here should be applicable to these spikelets as well: we predict them to resemble the second derivative of the AP in the nearby neurons [85], and to critically depend on contact area, but also on proximity and on the resistivity of the extracellular fluid.

We believe that the major reason for the lack of prespikes at most synapses is that the prespike amplitude is proportional to the 4th power of the synapse radius (Appendix B2). During the postnatal development of the MNTB, it can therefore be argued that the absence of postsynaptic recordings with multiple prespikes cannot be used as firm evidence against the presence of multiple calyces on these cells. We previously found anecdotal evidence for the presence of multiple large inputs during early postnatal development [86]. In a small fraction of the recordings multiple large inputs were observed, one with and one without a

prespike. It might be that the one without the prespike had a smaller surface area or a higher cleft height, going below the radar. This highly nonlinear dependence on apposition area may thus provide an explanation for the discrepancy between anatomical evidence favoring multiple large inputs during development [87] and the lack of recordings with multiple prespikes.

Divide and conquer

Virtually all synapses have in common that neurotransmission is initiated by a presynaptic action potential that results in capacitive cleft currents. The size of these currents depends on the amplitude and speed of the presynaptic AP. The properties of the presynaptic APs have mostly been studied at giant synapses, where they tend to be large and fast [46, 88-93]. These giant synapses are typically relay synapses that are specialized for rapid signaling, but recent measurements at more conventional bouton synapses in the neocortex show that their presynaptic action potentials are large and fast as well [94]. These capacitive currents, together with the presynaptic ion channel currents, will lead to a change in the cleft potential whose time course will closely follow the time course of the presynaptic membrane currents, and whose amplitude will critically depend on the cleft resistivity. Because of this cleft potential, the presynaptic ion channels facing the cleft will sense a reduced action potential. We showed that this should result in a less effective and delayed opening of the presynaptic calcium channels facing the synaptic cleft. Since rapid and large changes in the voltage sensed by the presynaptic ion channels serve to rapidly turn transmitter release on and off again, large cleft potentials seem undesirable, even though they may serve other, more beneficial functions such as influencing the neurotransmitter mobility within the cleft [15, 16], or rapidly inhibiting postsynaptic action potential generation [18, 95].

Above, we argued that many radial-like synapses should have a cleft conductance similar to what was measured here. An important difference between small and large synapses, however, is that the total current will be much larger in the large synapse, as the capacitive current scales with the presynaptic

apposition area. A large synapse thus has to dissipate this much larger current over a cleft conductance that is similar to the cleft conductance of a small synapse. There are three obvious different neural strategies to mitigate significant cleft potentials. Firstly, a strategy may be widenings of the synaptic cleft in between synaptic junctions. These intrasynaptic space enlargements [4], also called channels of extracellular spaces [96, 97] or subsynaptic cavities [98], have been found at many synapses, including the calyx of Held synapse, and may increase cleft conductance. Interestingly, a knockout of brevican, a component of the extracellular matrix of perineuronal nets, leads to a reduction of the size of the subsynaptic cavities at the calyx of Held synapse and an increased synaptic delay, even though the relation with a change in cleft conductance remains to be established [98]. The second strategy is to divide the cleft membrane currents over many postsynaptic junctions. For example, in the case of the squid giant synapse, the postsynaptic axon has numerous processes contacting the presynaptic axon, each with a width that is only ~1 μm [99]. At each of these processes the cleft potential will be small, thus effectively mitigating its impact. The last strategy is to fenestrate presynaptically. Most large synapses fenestrate presynaptically during development, leading to extended extracellular spaces [97]. Well-known examples include the neuromuscular junction, where the terminal arbor assumes a pretzel shape [100], the calyx of Held, which develops from a cup shape to the calyx shape [52, 53], the endbulb of Held synapse [54] or the avian ciliary ganglion [55]. In Appendix B5 we quantified the impact this will have on the size of the cleft potential change and on the prespike. Previously, other roles for these adaptations have been emphasized, such as speeding up of transmitter clearance or minimization of crosstalk between postsynaptic densities, both for the calyx of Held synapse [52, 101, 102] and at other synapses [103, 104]. The digitated adult morphology of the calyx of Held is accompanied by an increase in the number of puncta adhaerentia [102] and the formation of swellings connected via necks to the fingers [51, 105]. In the adult calyx of Held, a large fraction of the release takes place at these swellings, which should facilitate the dissipation of capacitive currents by the cleft, and reduce the impact of the cleft conductance on the postsynaptic currents.

In conclusion, we show here that the prespike of the calyx of Held synapse can be used to infer critical properties of its synaptic cleft; apart from the cleft conductance, it may also provide information about the presence or absence of ion channels at the cleft, or the effectiveness of morphological changes in reducing the size of cleft potentials during development. We thus provide a quantitative description for how the synaptic cleft, despite its narrow, limited space, can sustain the large and fast currents that are at the heart of chemical neurotransmission.

Materials & Methods

Analytical solutions for the transfer functions were derived using phasors. Analytical solutions for the Fourier transformation were checked using Wolfram Alpha. The derivations are outlined in Appendix A. Phasor calculations were done in Igor Pro 6.37 (WaveMetrics Inc., Lake Oswego, Oregon) using built-in functions: cmplx, FFT, IFFT and MatrixOP. The AP template shown in Figure 3A was based on an AP template previously used in voltage-clamp experiments [42] that was smoothed to eliminate the high-frequency oscillations that can arise after inverse Fourier transformation.

For the experimental procedures and recording conditions for the dual recordings of the calcium current and the postsynaptic currents, we refer the reader to the original paper [43]. *In vivo* whole-cell current-clamp recordings of developing MNTB principal neurons with afferent stimulation were previously reported in Sierksma, Slotman (37) (n = 6). *In vivo* whole-cell current-clamp recordings of MNTB principal neurons from adult C57BL/6J mice were previously reported in Wang, van Woerden (58) (n = 7, only wild-type animals) or in Lorteije, Rusu (59) (n=5). We also refer to these papers for the respective ethics statements.

For numerical simulations with voltage-gated channels the following two differential equations were defined:

$$c_{post}\frac{dv_{post}}{dt} = c_{cl}\frac{dv_{cl}}{dt} - g_{post}(v_{post} - v_{rest})$$

$$2c_{cl}\frac{dv_{cl}}{dt} = c_{cl}\left(\frac{dv_{pre}}{dt} + \frac{dv_{post}}{dt}\right) - g_{cl}v_{cl} + \sum g_{max}p_{open}(v_{pre} - v_{cl} - v_{channel})$$

Where g_{max} represents the maximal conductance of a voltage-gated channel, p_{open} the open probability of the voltage-gated channels, which is calculated using a multiple-state model (see below), and $v_{channel}$ the reversal potential of the voltage-gated channel. The reversal potentials were 50 mV, -90 mV, 40 mV and -70 mV for the sodium conductance, potassium conductance, calcium conductance, and the resting membrane potential of the postsynaptic neuron, respectively. v_{pre} was defined by an AP waveform.

Voltage-gated conductances were modeled with multiple states following Yang, Wang (106) except for the calcium conductance. In the models C indicates a closed state, O the open state and I the inactivated state. The sodium channel followed a five states-model, the high-threshold and low-threshold potassium channel were modeled as a six-states channel, and the calcium channel as a two-state channel for which the open probability was squared:

Five states-model: $$C_1 \underset{\beta}{\overset{2\alpha}{\rightleftarrows}} C_2 \underset{2\beta}{\overset{\alpha}{\rightleftarrows}} C_3 \underset{\delta}{\overset{\gamma}{\rightleftarrows}} O \underset{\epsilon}{\overset{\theta}{\rightleftarrows}} I$$

Six states-model: $$C_1 \underset{\beta}{\overset{4\alpha}{\rightleftarrows}} C_2 \underset{2\beta}{\overset{3\alpha}{\rightleftarrows}} C_3 \underset{3\beta}{\overset{2\alpha}{\rightleftarrows}} C_4 \underset{4\beta}{\overset{\alpha}{\rightleftarrows}} C_5 \underset{\delta}{\overset{\gamma}{\rightleftarrows}} O$$

Two states-model: $$C \underset{\beta}{\overset{\alpha}{\rightleftarrows}} O$$

The rate constants indicated by the Greek letters in the state models were calculated as

$$k = a\, e^{b(v_{pre} - v_{cl})}$$

where k represents a particular rate constant, and *a* and *b* are channel-specific parameters listed in Table 1. To take into account a possible effect of the cleft potential on the channel kinetics, the rate constant was calculated using the voltage difference between the presynaptic potential and the cleft potential.
The ordinary differential equations were numerically solved in Igor using IntegrateODE with default settings.

Statistics are reported as mean and standard deviation. Pearson's correlation coefficient was calculated to quantify correlations.

Table 1. Rate constants for the voltage-gated channels			
		a (ms^{-1})	**b (mV^{-1})**
Sodium conductance	**α**	48.9	1/128.4
	β	1.46	-1/8.9
	γ	392.8	1/36.0
	δ	0.73	-1/15.5
	ε	7.8	1/35.9
	θ	0.01	-1/18
High-threshold potassium conductance	**α**	1.097	1/57.404
	β	0.794	-1/79.264
	γ	33.750	0
	δ	74.360	0
Low-threshold potassium conductance	**α**	1.204	1/37.574
	β	0.360	-1/230
	γ	245.488	0
	δ	132.566	0
Calcium conductance	**α**	1.78	1/23.3
	β	0.14	-1/15
Parameters were taken from Yang, Wang (106), except for the calcium conductance [44].			

Acknowledgements

We thank Dr. Henrique von Gersdorff for helpful discussions on the developmental changes in the prespike.

References

1. Foster M. A text-book of physiology: Lea Brothers & Company; 1895.
2. Bennett MR. The early history of the synapse: from Plato to Sherrington. Brain Research Bulletin. 1999;50(2):95-118. doi: 10.1016/S0361-9230(99)00094-5.
3. Sotelo C. The history of the synapse. The Anatomical Record. 2020;303(5):1252-79. doi: 10.1002/ar.24392.
4. Palay SL. Synapses in the central nervous system. The Journal of Cell Biology. 1956;2(4):193-202. doi: 10.1083/jcb.2.4.193.
5. De Robertis E. Submicroscopic changes of the synapse after nerve section in the acoustic ganglion of the guinea pig; an electron microscope study. The Journal of Biophysical and Biochemical Cytology. 1956;2(5):503-12. doi: 10.1083/jcb.2.5.503.
6. Harris KM, Weinberg RJ. Ultrastructure of synapses in the mammalian brain. Cold Spring Harbor perspectives in biology. 2012;4(5):a005587. doi: 10.1101/cshperspect.a005587.
7. Eccles JC, Jaeger JC. The relationship between the mode of operation and the dimensions of the junctional regions at synapses and motor end-organs. Proceedings of the Royal Society of London Series B-Biological Sciences. 1958;148(930):38-56. doi: 10.1098/rspb.1958.0003.
8. Cho S, von Gersdorff H. Proton-mediated block of Ca^{2+} channels during multivesicular release regulates short-term plasticity at an auditory hair cell synapse. The Journal of Neuroscience. 2014;34(48):15877-87. doi: 10.1523/jneurosci.2304-14.2014.
9. DeVries SH. Exocytosed protons feedback to suppress the Ca^{2+} current in mammalian cone photoreceptors. Neuron. 2001;32(6):1107-17. doi: 10.1016/S0896-6273(01)00535-9.
10. Contini D, Price SD, Art JJ. Accumulation of K^+ in the synaptic cleft modulates activity by influencing both vestibular hair cell and calyx afferent in the turtle. The Journal of Physiology. 2017;595(3):777-803. doi: 10.1113/JP273060.
11. Goldberg JM. Theoretical analysis of intercellular communication between the vestibular type I hair cell and its calyx ending. Journal of Neurophysiology. 1996;76(3):1942-57. doi: 10.1152/jn.1996.76.3.1942. PubMed PMID: 8890305.
12. Shih PY, Savtchenko LP, Kamasawa N, Dembitskaya Y, McHugh TJ, Rusakov DA, et al. Retrograde synaptic signaling mediated by K^+ efflux through postsynaptic NMDA receptors. Cell Rep. 2013;5(4):941-51. doi: 10.1016/j.celrep.2013.10.026. PubMed PMID: 24268779.
13. Borst JGG, Sakmann B. Depletion of calcium in the synaptic cleft of a calyx-type synapse in the rat brainstem. Journal of Physiology. 1999;521:123-33. doi: 10.1111/j.1469-7793.1999.00123.x.
14. Stanley EF. Presynaptic calcium channels and the depletion of synaptic cleft calcium ions. J Neurophysiol. 2000;83(1):477-82. doi: 10.1152/jn.2000.83.1.477. PubMed PMID: 10634889.
15. Sylantyev S, Savtchenko LP, Niu Y-P, Ivanov AI, Jensen TP, Kullmann DM, et al. Electric fields due to synaptic currents sharpen excitatory transmission. Science. 2008;319(5871):1845-9. doi: 10.1126/science.1154330.
16. Savtchenko LP, Rusakov DA. The optimal height of the synaptic cleft. Proceedings of the National Academy of Sciences. 2007;104(6):1823. doi: 10.1073/pnas.0606636104.
17. Savtchenko LP, Poo MM, Rusakov DA. Electrodiffusion phenomena in neuroscience: a neglected companion. Nat Rev Neurosci. 2017;18(10):598-612. doi: 10.1038/nrn.2017.101. PubMed PMID: 28924257.
18. Blot A, Barbour B. Ultra-rapid axon-axon ephaptic inhibition of cerebellar Purkinje cells by the pinceau. Nat Neurosci. 2014;17(2):289-95. Epub 2014/01/15. doi: 10.1038/nn.3624. PubMed PMID: 24413696.

657 19. Rusakov DA, Savtchenko LP, Zheng K, Henley JM. Shaping the synaptic signal: molecular mobility
658 inside and outside the cleft. Trends in Neurosciences. 2011;34(7):359-69. doi:
659 10.1016/j.tins.2011.03.002.
660 20. Savtchenko LP, Antropov SN, Korogod SM. Effect of voltage drop within the synaptic cleft on the
661 current and voltage generated at a single synapse. Biophysical Journal. 2000;78(3):1119-25. doi:
662 10.1016/S0006-3495(00)76670-7.
663 21. Berretta N, Rossokhin AV, Kasyanov AM, Sokolov MV, Cherubini E, Voronin LL. Postsynaptic
664 hyperpolarization increases the strength of AMPA-mediated synaptic transmission at large synapses
665 between mossy fibers and CA3 pyramidal cells. Neuropharmacology. 2000;39(12):2288-301. doi:
666 10.1016/s0028-3908(00)00076-9. PubMed PMID: 10974312.
667 22. Faber DS, Funch PG. Differential properties of orthodromic and antidromic impulse propagation
668 across the Mauthner cell initial segment. Brain Research. 1980;190(1):255-60. doi: 10.1016/0006-
669 8993(80)91176-2.
670 23. del Castillo J, Katz B. Localization of active spots within the neuromuscular junction of the frog.
671 The Journal of Physiology. 1956;132(3):630-49. doi: 10.1113/jphysiol.1956.sp005554.
672 24. Martin AR, Pilar G. An analysis of electrical coupling at synapses in the avian ciliary ganglion. J
673 Physiol. 1964;171:454-75. doi: 10.1113/jphysiol.1964.sp007390. PubMed PMID: 14193934; PubMed
674 Central PMCID: PMCPMC1368844.
675 25. Dmitriev AV, Mangel SC. Electrical feedback in the cone pedicle: A computational analysis.
676 Journal of Neurophysiology. 2006;95(3):1419-27. doi: 10.1152/jn.00098.2005. PubMed PMID: 16319220.
677 26. Fahrenfort I, Steijaert M, Sjoerdsma T, Vickers E, Ripps H, van Asselt J, et al. Hemichannel-
678 mediated and pH-based feedback from horizontal cells to cones in the vertebrate retina. PLoS One.
679 2009;4(6):e6090. doi: 10.1371/journal.pone.0006090. PubMed PMID: 19564917; PubMed Central
680 PMCID: PMCPMC2699542.
681 27. Kamermans M, Fahrenfort I, Schultz K, Janssen-Bienhold U, Sjoerdsma T, Weiler R. Hemichannel-
682 mediated inhibition in the outer retina. Science. 2001;292(5519):1178-80. doi: 10.1126/science.1060101.
683 PubMed PMID: 11349152.
684 28. Kasyanov AM, Maximov VV, Byzov AL, Berretta N, Sokolov MV, Gasparini S, et al. Differences in
685 amplitude-voltage relations between minimal and composite mossy fibre responses of rat CA3
686 hippocampal neurons support the existence of intrasynaptic ephaptic feedback in large synapses.
687 Neuroscience. 2000;101(2):323-36. doi: 10.1016/S0306-4522(00)00366-3. PubMed PMID: 11074156.
688 29. Byzov AL, Shura-Bura TM. Electrical feedback mechanism in the processing of signals in the outer
689 plexiform layer of the retina. Vision Res. 1986;26(1):33-44. doi: 10.1016/0042-6989(86)90069-6. PubMed
690 PMID: 3012877.
691 30. Savtchenko LP. Bilateral processing in chemical synapses with electrical 'ephaptic' feedback: a
692 theoretical model. Math Biosci. 2007;207(1):113-37. doi: 10.1016/j.mbs.2006.09.016. PubMed PMID:
693 17112549.
694 31. Morest DK. The growth of synaptic endings in the mammalian brain: a study of the calyces of the
695 trapezoid body. Zeitschrift für Anatomie und Entwicklungsgeschichte. 1968;127(3):201-20. doi:
696 10.1007/BF00526129.
697 32. Rollenhagen A, Lübke JHR. The morphology of excitatory central synapses: from structure to
698 function. Cell Tissue Res. 2006;326(2):221-37. doi: 10.1007/s00441-006-0288-z. PubMed PMID:
699 16932936.
700 33. Borst JGG, Soria van Hoeve J. The calyx of Held synapse: from model synapse to auditory relay.
701 Annual Review of Physiology. 2012;74:199-224. Epub 2011/11/01. doi: 10.1146/annurev-physiol-
702 020911-153236. PubMed PMID: 22035348.

703 34. Forsythe ID. Direct patch recording from identified presynaptic terminals mediating
704 glutamatergic EPSCs in the rat CNS, *in vitro*. J Physiol. 1994;479(3):381-7. doi:
705 10.1113/jphysiol.1994.sp020303.
706 35. von Gersdorff H, Borst JGG. Short-term plasticity at the calyx of Held. Nature Reviews
707 Neuroscience. 2002;3:53-64.
708 36. Borst JGG, Helmchen F, Sakmann B. Pre- and postsynaptic whole-cell recordings in the medial
709 nucleus of the trapezoid body of the rat. J Physiol. 1995;489(Pt 3):825-40. doi:
710 10.1113/jphysiol.1995.sp021095.
711 37. Sierksma MC, Slotman JA, Houtsmuller AB, Borst JGG. Structure–function relation of the
712 developing calyx of Held synapse *in vivo*. The Journal of Physiology. 2020;598(20):4603-19. doi:
713 10.1113/JP279976.
714 38. Korogod N, Petersen CCH, Knott GW. Ultrastructural analysis of adult mouse neocortex
715 comparing aldehyde perfusion with cryo fixation. Elife. 2015;4. doi: 10.7554/eLife.05793. PubMed PMID:
716 26259873; PubMed Central PMCID: PMCPMC4530226.
717 39. Syková E, Nicholson C. Diffusion in brain extracellular space. Physiol Rev. 2008;88(4):1277-340.
718 doi: 10.1152/physrev.00027.2007. PubMed PMID: 18923183.
719 40. Rubio ME, Nagy JI. Connexin36 expression in major centers of the auditory system in the CNS of
720 mouse and rat: Evidence for neurons forming purely electrical synapses and morphologically mixed
721 synapses. Neuroscience. 2015;303:604-29. Epub 2015/07/19. doi: 10.1016/j.neuroscience.2015.07.026.
722 PubMed PMID: 26188286; PubMed Central PMCID: PMC4576740.
723 41. Meinrenken CJ, Borst JGG, Sakmann B. Calcium secretion coupling at calyx of Held governed by
724 nonuniform channel-vesicle topography. J Neurosci. 2002;22(5):1648-67. doi: 10.1523/JNEUROSCI.22-05-
725 01648.2002. PubMed PMID: 11880495.
726 42. Borst JGG, Sakmann B. Calcium influx and transmitter release in a fast CNS synapse. Nature.
727 1996;383(6599):431-4. doi: 10.1038/383431a0.
728 43. Borst JGG, Sakmann B. Effect of changes in action potential shape on calcium currents and
729 transmitter release in a calyx-type synapse of the rat auditory brainstem. Philos Trans R Soc Lond B Biol
730 Sci. 1999;354(1381):347-55. doi: 10.1098/rstb.1999.0386. PubMed PMID: 10212483.
731 44. Borst JGG, Sakmann B. Calcium current during a single action potential in a large presynaptic
732 terminal of the rat brainstem. J Physiol. 1998;506:143-57. doi: 10.1111/j.1469-7793.1998.143bx.x.
733 45. Wu L-G, Westenbroek RE, Borst JGG, Catterall WE, Sakmann B. Calcium channel types with
734 distinct presynaptic localization couple differentially to transmitter release in single calyx-type synapses.
735 Journal of Neuroscience. 1999;19:726-36. doi: 10.1523/JNEUROSCI.19-02-00726.1999
736 46. Taschenberger H, von Gersdorff H. Fine-tuning an auditory synapse for speed and fidelity:
737 developmental changes in presynaptic waveform, EPSC kinetics, and synaptic plasticity. J Neurosci.
738 2000;20(24):9162-73. doi: 10.1523/JNEUROSCI.20-24-09162.2000 PubMed PMID: 11124994.
739 47. Barnes-Davies M, Forsythe ID. Pre- and postsynaptic glutamate receptors at a giant excitatory
740 synapse in rat auditory brainstem slices. Journal of Physiology. 1995;488(2):387-406. doi:
741 10.1113/jphysiol.1995.sp020974.
742 48. Forsythe ID, Barnes-Davies M. The binaural auditory pathway: excitatory amino acid receptors
743 mediate dual timecourse excitatory postsynaptic currents in the rat medial nucleus of the trapezoid
744 body. Proceedings of the Royal Society B. 1993;251(1331):151-7. doi: 10.1098/rspb.1993.0022.
745 49. Joshi I, Wang L-Y. Developmental profiles of glutamate receptors and synaptic transmission at a
746 single synapse in the mouse auditory brainstem. J Physiol. 2002;540(Pt 3):861-73. doi:
747 10.1113/jphysiol.2001.013506. PubMed PMID: 11986375.
748 50. Sätzler K, Söhl LF, Bollmann JH, Borst JGG, Frotscher M, Sakmann B, et al. Three-dimensional
749 reconstruction of a calyx of Held and its postsynaptic principal neuron in the medial nucleus of the
750 trapezoid body. J Neurosci. 2002;22(24):10567-79. PubMed PMID: 12486149.

751 51. Rowland KC, Irby NK, Spirou GA. Specialized synapse-associated structures within the calyx of
752 Held. J Neurosci. 2000;20(24):9135-44. doi: 10.1523/JNEUROSCI.20-24-09135.2000. PubMed PMID:
753 11124991.
754 52. Ford MC, Grothe B, Klug A. Fenestration of the calyx of Held occurs sequentially along the
755 tonotopic axis, is influenced by afferent activity, and facilitates glutamate clearance. J Comp Neurol.
756 2009;514(1):92-106. PubMed PMID: 19260071.
757 53. Kandler K, Friauf E. Pre- and postnatal development of efferent connections of the cochlear
758 nucleus in the rat. Journal of Comparative Neurology. 1993;328(2):161-84. doi: 10.1002/cne.903280202.
759 54. Ryugo DK, Montey KL, Wright AL, Bennett ML, Pongstaporn T. Postnatal development of a large
760 auditory nerve terminal: the endbulb of Held in cats. Hear Res. 2006;216-217:100-15. Epub 2006/02/25.
761 doi: 10.1016/j.heares.2006.01.007. PubMed PMID: 16497457.
762 55. Hess A, Pilar G, Weakly JN. Correlation between transmission and structure in avian ciliary
763 ganglion synapses. J Physiol. 1969;202(2):339-54. doi: 10.1113/jphysiol.1969.sp008815. PubMed PMID:
764 4306543; PubMed Central PMCID: PMCPMC1351486.
765 56. Baydyuk M, Xu J, Wu LG. The calyx of Held in the auditory system: Structure, function, and
766 development. Hear Res. 2016;338:22-31. Epub 2016/03/29. doi: 10.1016/j.heares.2016.03.009. PubMed
767 PMID: 27018297; PubMed Central PMCID: PMC4967386.
768 57. Spirou GA, Chirila FV, von Gersdorff H, Manis PB. Heterogeneous Ca^{2+} influx along the adult calyx
769 of Held: a structural and computational study. Neuroscience. 2008;154(1):171-85. PubMed PMID:
770 18485608.
771 58. Wang T, van Woerden GM, Elgersma Y, Borst JGG. Enhanced transmission at the calyx of Held
772 synapse in a mouse model for Angelman syndrome. Front Cell Neurosci. 2017;11:418. Epub 2018/01/23.
773 doi: 10.3389/fncel.2017.00418. PubMed PMID: 29354033; PubMed Central PMCID: PMC5758499.
774 59. Lorteije JAM, Rusu SI, Kushmerick C, Borst JGG. Reliability and precision of the mouse calyx of
775 Held synapse. J Neurosci. 2009;29(44):13770-84. doi: 10.1523/JNEUROSCI.3285-09.2009. PubMed PMID:
776 19889989.
777 60. Leão RM, Kushmerick C, Pinaud R, Renden R, Li G-L, Taschenberger H, et al. Presynaptic Na^{+}
778 channels: locus, development, and recovery from inactivation at a high-fidelity synapse. J Neurosci.
779 2005;25(14):3724-38. doi: 10.1523/JNEUROSCI.3983-04.2005. PubMed PMID: 15814803.
780 61. Yang Y-M, Wang L-Y. Amplitude and kinetics of action potential-evoked Ca^{2+} current and its
781 efficacy in triggering transmitter release at the developing calyx of Held synapse. J Neurosci.
782 2006;26(21):5698-708. doi: 10.1523/JNEUROSCI.4889-05.2006 PubMed PMID: 16723526.
783 62. Fekete A, Nakamura Y, Yang YM, Herlitze S, Mark MD, DiGregorio DA, et al. Underpinning
784 heterogeneity in synaptic transmission by presynaptic ensembles of distinct morphological modules. Nat
785 Commun. 2019;10(1):826. Epub 2019/02/20. doi: 10.1038/s41467-019-08452-2. PubMed PMID:
786 30778063; PubMed Central PMCID: PMC6379440.
787 63. Martin AR, Pilar G. Transmission through the ciliary ganglion of the chick. Journal of Physiology.
788 1963;168:464-75.
789 64. Funch PG, Faber DS. Action-potential propagation and orthodromic impulse initiation in
790 Mauthner axon. Journal of Neurophysiology. 1982;47(6):1214-31. doi: 10.1152/jn.1982.47.6.1214
791 65. Vandenbranden CA, Verweij J, Kamermans M, Muller LJ, Ruijter JM, Vrensen GF, et al. Clearance
792 of neurotransmitter from the cone synaptic cleft in goldfish retina. Vision Research. 1996;36(24):3859-
793 74. doi: 10.1016/s0042-6989(96)00134-4.
794 66. DeVries SH, Li W, Saszik S. Parallel processing in two transmitter microenvironments at the cone
795 photoreceptor synapse. Neuron. 2006;50(5):735-48. doi: 10.1016/j.neuron.2006.04.034. PubMed PMID:
796 16731512.

797 67. Baumann SB, Wozny DR, Kelly SK, Meno FM. The electrical conductivity of human cerebrospinal
798 fluid at body temperature. IEEE Trans Biomed Eng. 1997;44(3):220-3. doi: 10.1109/10.554770. PubMed
799 PMID: 9216137.
800 68. Roth A, Häusser M. Compartmental models of rat cerebellar Purkinje cells based on
801 simultaneous somatic and dendritic patch-clamp recordings. J Physiol. 2001;535(Pt 2):445-72. doi:
802 10.1111/j.1469-7793.2001.00445.x. PubMed PMID: 11533136.
803 69. Golding NL, Mickus TJ, Katz Y, Kath WL, Spruston N. Factors mediating powerful voltage
804 attenuation along CA1 pyramidal neuron dendrites. J Physiol. 2005;568(Pt 1):69-82. doi:
805 10.1113/jphysiol.2005.086793. PubMed PMID: 16002454; PubMed Central PMCID: PMCPMC1474764.
806 70. Cohen CCH, Popovic MA, Klooster J, Weil MT, Mobius W, Nave KA, et al. Saltatory conduction
807 along myelinated axons involves a periaxonal nanocircuit. Cell. 2020;180(2):311-22 e15. doi:
808 10.1016/j.cell.2019.11.039. PubMed PMID: 31883793; PubMed Central PMCID: PMCPMC6978798.
809 71. Zheng K, Jensen TP, Savtchenko LP, Levitt JA, Suhling K, Rusakov DA. Nanoscale diffusion in the
810 synaptic cleft and beyond measured with time-resolved fluorescence anisotropy imaging. Scientific
811 Reports. 2017;7(1):42022. doi: 10.1038/srep42022.
812 72. Land BR, Harris WV, Salpeter EE, Salpeter MM. Diffusion and binding constants for acetylcholine
813 derived from the falling phase of miniature endplate currents. Proc Natl Acad Sci U S A. 1984;81(5):1594-
814 8. doi: 10.1073/pnas.81.5.1594. PubMed PMID: 6584895; PubMed Central PMCID: PMCPMC344884.
815 73. Faber DS, Funch PG, Korn H. Evidence that receptors mediating central synaptic potentials
816 extend beyond the postsynaptic density. Proc Natl Acad Sci U S A. 1985;82(10):3504-8. doi:
817 10.1073/pnas.82.10.3504. PubMed PMID: 2582417; PubMed Central PMCID: PMCPMC397805.
818 74. Nielsen TA, DiGregorio DA, Silver RA. Modulation of glutamate mobility reveals the mechanism
819 underlying slow-rising AMPAR EPSCs and the diffusion coefficient in the synaptic cleft. Neuron.
820 2004;42(5):757-71. doi: 10.1016/j.neuron.2004.04.003. PubMed PMID: 15182716.
821 75. Guinan JJ, Jr., Li RY-S. Signal processing in brainstem auditory neurons which receive giant
822 endings (calyces of Held) in the medial nucleus of the trapezoid body of the cat. Hear Res. 1990;49(1-
823 3):321-34. doi: 10.1016/0378-5955(90)90111-2.
824 76. Pfeiffer RR. Anteroventral cochlear nucleus: wave forms of extracellularly recorded spike
825 potentials. Science. 1966;154(749):667-8. doi: 10.1126/science.154.3749.667 PubMed PMID: 5923782.
826 77. Typlt M, Haustein MD, Dietz B, Steinert JR, Witte M, Englitz B, et al. Presynaptic and postsynaptic
827 origin of multicomponent extracellular waveforms at the endbulb of Held-spherical bushy cell synapse.
828 Eur J Neurosci. 2010;31(9):1574-81. Epub 2010/06/09. doi: 10.1111/j.1460-9568.2010.07188.x. PubMed
829 PMID: 20525070.
830 78. Eysel UT. Quantitative studies of intracellular postsynaptic potentials in the lateral geniculate
831 nucleus of the cat with respect to optic tract stimulus response latencies. Exp Brain Res. 1976;25:469-86.
832 doi: 10.1007/bf00239782. PubMed PMID: 182514.
833 79. Dudel J. Effect of inhibition on the presynaptic nerve terminal in the neuromuscular junction of
834 the crayfish. Nature. 1962;193:587-8. doi: 10.1038/193587b0. PubMed PMID: 13888196.
835 80. Takeuchi A, Takeuchi N. Electrical changes in pre- and postsynaptic axons of the giant synapse of
836 Loligo. J Gen Physiol. 1962;45:1181-93. doi: 10.1085/jgp.45.6.1181. PubMed PMID: 13919241; PubMed
837 Central PMCID: PMCPMC2195243.
838 81. Katz B, Miledi R. Propagation of electric activity in motor nerve terminals. Proceedings of the
839 Royal Society B. 1965;161:453-82. doi: 10.1098/rspb.1965.0015.
840 82. Mathy A, Ho SSN, Davie JT, Duguid IC, Clark BA, Häusser M. Encoding of oscillations by axonal
841 bursts in inferior olive neurons. Neuron. 2009;62(3):388-99. Epub 2009/05/19. doi:
842 10.1016/j.neuron.2009.03.023. PubMed PMID: 19447094; PubMed Central PMCID: PMC2777250.

843 83. Maruta J, Hensbroek RA, Simpson JI. Intraburst and interburst signaling by climbing fibers. J
844 Neurosci. 2007;27(42):11263-70. Epub 2007/10/19. doi: 10.1523/JNEUROSCI.2559-07.2007. PubMed
845 PMID: 17942720.
846 84. Michalikova M, Remme MWH, Schmitz D, Schreiber S, Kempter R. Spikelets in pyramidal
847 neurons: generating mechanisms, distinguishing properties, and functional implications. Rev Neurosci.
848 2019;31(1):101-19. doi: 10.1515/revneuro-2019-0044. PubMed PMID: 31437125.
849 85. Vigmond EJ, Perez Velazquez JL, Valiante TA, Bardakjian BL, Carlen PL. Mechanisms of electrical
850 coupling between pyramidal cells. J Neurophysiol. 1997;78(6):3107-16. doi: 10.1152/jn.1997.78.6.3107.
851 PubMed PMID: 9405530.
852 86. Sierksma MC, Tedja MS, Borst JGG. *In vivo* matching of postsynaptic excitability with
853 spontaneous synaptic inputs during formation of the rat calyx of Held synapse. J Physiol.
854 2016;595(1):207-31. Epub 2016/07/19. doi: 10.1113/JP272780. PubMed PMID: 27426483.
855 87. Holcomb PS, Hoffpauir BK, Hoyson MC, Jackson DR, Deerinck TJ, Marrs GS, et al. Synaptic inputs
856 compete during rapid formation of the calyx of Held: a new model system for neural development. J
857 Neurosci. 2013;33(32):12954-69. Epub 2013/08/09. doi: 10.1523/JNEUROSCI.1087-13.2013. PubMed
858 PMID: 23926251; PubMed Central PMCID: PMC3735879.
859 88. Ritzau-Jost A, Delvendahl I, Rings A, Byczkowicz N, Harada H, Shigemoto R, et al. Ultrafast action
860 potentials mediate kilohertz signaling at a central synapse. Neuron. 2014;84(1):152-63. doi:
861 10.1016/j.neuron.2014.08.036.
862 89. Sierksma MC, Borst JGG. Resistance to action potential depression of a rat axon terminal in vivo.
863 Proc Natl Acad Sci U S A. 2017;114(16):4249-54. Epub 2017/04/05. doi: 10.1073/pnas.1619433114.
864 PubMed PMID: 28373550; PubMed Central PMCID: PMC5402426.
865 90. Lin KH, Oleskevich S, Taschenberger H. Presynaptic Ca^{2+} influx and vesicle exocytosis at the
866 mouse endbulb of Held: a comparison of two auditory nerve terminals. J Physiol. 2011;589(17):4301-20.
867 doi: 10.1113/jphysiol.2011.209189. PubMed PMID: 21746778; PubMed Central PMCID:
868 PMCPMC3180584.
869 91. Rancz EA, Ishikawa T, Duguid I, Chadderton P, Mahon S, Häusser M. High-fidelity transmission of
870 sensory information by single cerebellar mossy fibre boutons. Nature. 2007;450(7173):1245-8. doi:
871 10.1038/nature05995. PubMed PMID: 18097412.
872 92. Geiger JR, Jonas P. Dynamic control of presynaptic Ca^{2+} inflow by fast-inactivating K^{+} channels in
873 hippocampal mossy fiber boutons. Neuron. 2000;28(3):927-39. PubMed PMID: 11163277.
874 93. Bischofberger J, Geiger JRP, Jonas P. Timing and efficacy of Ca^{2+} channel activation in
875 hippocampal mossy fiber boutons. J Neurosci. 2002;22(24):10593-602. Epub 2002/12/18. doi:
876 10.1523/JNEUROSCI.22-24-10593.2002 PubMed PMID: 12486151.
877 94. Ritzau-Jost A, Tsintsadze T, Krueger M, Ader J, Bechmann I, Eilers J, et al. Large, stable spikes
878 exhibit differential broadening in excitatory and inhibitory neocortical boutons. Cell Rep.
879 2021;34(2):108612. doi: 10.1016/j.celrep.2020.108612. PubMed PMID: 33440142; PubMed Central
880 PMCID: PMCPMC7809622.
881 95. Furukawa T, Furshpan EJ. Two inhibitory mechanisms in the Mauthner neurons of goldfish. J
882 Neurophysiol. 1963;26:140-76. doi: 10.1152/jn.1963.26.1.140. PubMed PMID: 13945908.
883 96. Tatsuoka H, Reese TS. New structural features of synapses in the anteroventral cochlear nucleus
884 prepared by direct freezing and freeze-substitution. Journal of Comparative Neurology. 1989;290(3):343-
885 57. doi: 10.1002/cne.902900304.
886 97. Nakajima Y. Fine structure of the medial nucleus of the trapezoid body of the bat with special
887 reference to two types of synaptic endings. J Cell Biol. 1971;50(1):121-34. doi: 10.1083/jcb.50.1.121
888 98. Blosa M, Sonntag M, Jäger C, Weigel S, Seeger J, Frischknecht R, et al. The extracellular matrix
889 molecule brevican is an integral component of the machinery mediating fast synaptic transmission at the

890 calyx of Held. J Physiol. 2015;593(19):4341-60. Epub 2015/08/01. doi: 10.1113/jp270849. PubMed PMID:
891 26223835.
892 99. Martin R, Miledi R. The form and dimensions of the giant synapse of squids. Philosophical
893 Transactions of the Royal Society B. 1986;312(1155):355-77. doi: 10.1098/rstb.1986.0013.
894 100. Sanes JR, Lichtman JW. Development of the vertebrate neuromuscular junction. Annu Rev
895 Neurosci. 1999;22:389-442. Epub 1999/04/15. doi: 10.1146/annurev.neuro.22.1.389. PubMed PMID:
896 10202544.
897 101. Renden R, Taschenberger H, Puente N, Rusakov DA, Duvoisin R, Wang L-Y, et al. Glutamate
898 transporter studies reveal the pruning of metabotropic glutamate receptors and absence of AMPA
899 receptor desensitization at mature calyx of Held synapses. J Neurosci. 2005;25(37):8482-97. doi:
900 10.1523/JNEUROSCI.1848-05.2005. PubMed PMID: 16162930.
901 102. Taschenberger H, Leão RM, Rowland KC, Spirou GA, von Gersdorff H. Optimizing synaptic
902 architecture and efficiency for high-frequency transmission. Neuron. 2002;36(6):1127-43. doi:
903 10.1016/S0896-6273(02)01137-6. PubMed PMID: 12495627.
904 103. Graydon CW, Cho S, Diamond JS, Kachar B, von Gersdorff H, Grimes WN. Specialized
905 postsynaptic morphology enhances neurotransmitter dilution and high-frequency signaling at an
906 auditory synapse. J Neurosci. 2014;34(24):8358-72. doi: 10.1523/JNEUROSCI.4493-13.2014. PubMed
907 PMID: 24920639; PubMed Central PMCID: PMCPMC4051984.
908 104. Cathala L, Holderith NB, Nusser Z, DiGregorio DA, Cull-Candy SG. Changes in synaptic structure
909 underlie the developmental speeding of AMPA receptor-mediated EPSCs. Nat Neurosci.
910 2005;8(10):1310-8. doi: 10.1038/nn1534. PubMed PMID: 16172604.
911 105. Wimmer VC, Horstmann H, Groh A, Kuner T. Donut-like topology of synaptic vesicles with a
912 central cluster of mitochondria wrapped into membrane protrusions: a novel structure-function module
913 of the adult calyx of Held. J Neurosci. 2006;26(1):109-16. doi: 10.1523/JNEUROSCI.3268-05.2006
914 PubMed PMID: 16399677.
915 106. Yang YM, Wang W, Fedchyshyn MJ, Zhou Z, Ding J, Wang LY. Enhancing the fidelity of
916 neurotransmission by activity-dependent facilitation of presynaptic potassium currents. Nat Commun.
917 2014;5:4564. Epub 2014/08/01. doi: 10.1038/ncomms5564. PubMed PMID: 25078759.
918 107. Borst JGG, Helmchen F. Calcium influx during an action potential. In: Conn PM, editor. Methods
919 in Enzymology. Ion Channels. 293: Academic Press; 1998. p. 352-71.

920

Appendix A. Phasors

For the circuit shown in Figure 2, we assume the presence of a voltage oscillator at the calyx. For simplicity, we also assume that the admittances Y_1 and Y_4 of the resistive membrane components are small compared to the admittances Y_2 and Y_5 of the capacitive components and can therefore both be neglected. However, following the logic of the solutions below, it should be straightforward to derive the solution for a situation that also includes either or both resistive components.

Question A1: How does the cleft potential depend upon the presynaptic membrane potential?

The admittances surrounding the cleft form a voltage divider. We assume that the impact of the prespike at the postsynaptic cell is very small ($Y_5 >> Y_6$ or Y_7), so we can neglect the contribution of Y_6 and Y_7:

$$\frac{V_{cleft}}{V_{pre}} = \frac{-jY_2}{\mathrm{Y}_3 - j(\mathrm{Y}_2 + \mathrm{Y}_5)} = \frac{-jY_2}{\mathrm{Y}_3 - j(\mathrm{Y}_2 + \mathrm{Y}_5)} \frac{\mathrm{Y}_3 + j(\mathrm{Y}_2 + \mathrm{Y}_5)}{\mathrm{Y}_3 + j(\mathrm{Y}_2 + \mathrm{Y}_5)}$$

$$= \frac{Y_2}{{Y_3}^2 + (\mathrm{Y}_2 + \mathrm{Y}_5)^2} \left((Y_2 + Y_5) - jY_3\right) \qquad \text{(A1.1)}$$

This notation can be converted to the modulus:

$$\left|\frac{V_{cleft}}{V_{pre}}\right| = \frac{Y_2}{{Y_3}^2 + (\mathrm{Y}_2 + \mathrm{Y}_5)^2} \sqrt{(Y_2 + Y_5)^2 + {Y_3}^2} = \frac{Y_2}{\sqrt{(Y_2 + Y_5)^2 + {Y_3}^2}} \qquad \text{(A1.2)}$$

And a phase shift:

$$\varphi_f = atan2(-Y_3\,, (\,Y_2 + Y_5)) \qquad \text{(A1.3)}$$

If we assume that the pre- and the postsynaptic capacitance facing the cleft are identical (Y_2=Y_5):

$$\left|\frac{V_{cleft}}{V_{pre}}\right| = \frac{2\pi f c_{cl}}{\sqrt{(4\pi f c_{cl})^2 + {g_{cl}}^2}} \qquad \text{(A1.4)}$$

$$\varphi_f = atan2(-g_3\,, 4\pi f c_{cl}) \qquad \text{(A1.5)}$$

This can be simplified if $(4\pi f c_{cl})^2 \ll g_3^2$, which gives:

$$\left|\frac{V_{cleft}}{V_{pre}}\right| \leq \frac{2\pi f c_{cl}}{g_{cl}} = 2\pi f \tau_{cl} \qquad \text{(A1.6)}$$

The phase shift would approach –π/2, which reflects the first derivative of v_{pre}.

Question A2: how does the VC prespike depend on the passive synaptic parameters?

The current that flows into the synaptic cleft from the terminal will either leak away via the cleft conductance or enter into the postsynaptic cell. The current into the postsynaptic cell (i_{post}) can be described by:

$$I_{post} = -jY_5 V_{cleft} \;=\; -jY_5 \frac{-jY_2}{\mathrm{Y}_3 - \mathrm{j}(\mathrm{Y}_2 + \mathrm{Y}_5)} \mathrm{V}_{\mathrm{pre}} \qquad \text{(A2.1)}$$

$$\frac{I_{post}}{V_{pre}} = \frac{-Y_2 Y_5}{\mathrm{Y}_3 - \mathrm{j}(\mathrm{Y}_2 + \mathrm{Y}_5)} = \frac{Y_2 Y_5}{{Y_3}^2 + (\mathrm{Y}_2 + \mathrm{Y}_5)^2}\left(-\mathrm{Y}_3 - \mathrm{j}(\mathrm{Y}_2 + \mathrm{Y}_5)\right) \qquad \text{(A2.2)}$$

We then get:

$$\left|\frac{I_{post}}{V_{pre}}\right| = Y_2 Y_5 \frac{\sqrt{Y_3^2 + (Y_2 + Y_5)^2}}{{Y_3}^2 + (\mathrm{Y}_2 + \mathrm{Y}_5)^2} = \frac{Y_2 Y_5}{\sqrt{Y_3^2 + (Y_2 + Y_5)^2}} \qquad \text{(A2.3)}$$

If we assume that the pre- and postsynaptic cleft capacitance are the same (Y_2=Y_5):

$$\left|\frac{I_{post}}{V_{pre}}\right| = \frac{(2\pi f c_{cl})^2}{\sqrt{(4\pi f c_{cl})^2 + g_{cl}^2}} \qquad \text{(A2.4)}$$

$$\varphi_f = atan2(-(Y_2 + Y_5)\,, -Y_3) = atan2(-4\pi f c_{cl}, -g_{cl}) \qquad \text{(A2.5)}$$

Again, we may approximate the modulus by simplifying the equation to:

$$\left|\frac{I_{post}}{V_{pre}}\right| \leq \frac{(2\pi f c_{cl})^2}{g_{cl}} = g_{cl}(2\pi f \tau_{cl})^2 \qquad \text{(A2.6)}$$

Question A3: what is the equation for the CC prespike?

The postsynaptic voltage response can be described by i_{post} divided by the combinations of the different routes to the reference:

$$V_{post} = \frac{-I_{post}}{Y_{to\ the\ cleft} + Y_6 - jY_7} = \frac{-I_{post}}{({Y_3}^{-1} + (Y_4 - jY_5)^{-1})^{-1} + Y_6 - jY_7} \qquad \text{(A3.1)}$$

Here, we already assumed that none of the currents will reenter the calyx. As the cleft leak conductance is likely to be much higher than the cleft-facing admittance of the postsynaptic membrane ($Y_3^{-1} \ll (Y_4 - jY_5)^{-1}$), we get:

$$V_{post} = \frac{-I_{post}}{Y_4 - jY_5 + Y_6 - jY_7}$$

$$= \frac{-jY_5 V_{cleft}}{Y_4 - jY_5 + Y_6 - jY_7}$$

$$= \frac{1}{Y_4 - jY_5 + Y_6 - jY_7} \frac{-Y_2 Y_5}{\mathrm{Y}_3 - \mathrm{j}(\mathrm{Y}_2 + \mathrm{Y}_5)} V_{pre} \qquad \text{(A3.2)}$$

$$\frac{V_{post}}{V_{pre}} = \frac{-Y_2 Y_5}{(Y_4 + Y_6 - j(Y_5 + Y_7))(\mathrm{Y}_3 - \mathrm{j}(\mathrm{Y}_2 + \mathrm{Y}_5))} \qquad \text{(A3.3)}$$

To simplify the derivation, we combine Y_4+Y_6 to be the total postsynaptic conductance g_{post}, and we combine Y_5 + Y_7 to be the total postsynaptic susceptance $2\pi f c_{post}$:

$$\frac{V_{post}}{V_{pre}} = \frac{-Y_2 Y_5}{(g_{post} - j2\pi f c_{post})(Y_3 - j(\mathrm{Y}_2 + \mathrm{Y}_5)}$$

$$= \frac{Y_2 Y_5}{\left({g_{post}}^2 + \left(2\pi f c_{post}\right)^2\right)(Y_3^2 + (Y_2 + Y_5)^2)} \Big(-g_{post} Y_3 + 2\pi f c_{post}(Y_2 + Y_5)$$

$$- j\left(2\pi f c_{post} Y_3 + g_{post}(Y_2 + Y_5)\right)\Big) \quad \text{(A3.4)}$$

From this we can deduce the modulus:

$$\left|\frac{V_{post}}{V_{pre}}\right| = \frac{Y_2 Y_5 \sqrt{\left(2\pi f c_{post}(Y_2+Y_5) - g_{post}Y_3\right)^2 + \left(2\pi f c_{post}Y_3 + g_{post}(Y_2+Y_5)\right)^2}}{\left({g_{post}}^2 + \left(2\pi f c_{post}\right)^2\right)(Y_3^2 + (Y_2+Y_5)^2)}$$

$$= \frac{Y_2 Y_5}{\sqrt{\left({g_{post}}^2 + \left(2\pi f c_{post}\right)^2\right)(Y_3^2 + (Y_2+Y_5)^2)}} \quad \text{(A3.5)}$$

Assuming again that the susceptance towards the synaptic cleft ($Y_2 = Y_5$) is the same:

$$\left|\frac{V_{post}}{V_{pre}}\right| = \frac{(2\pi f c_{cl})^2}{\sqrt{\left({g_{post}}^2 + \left(2\pi f c_{post}\right)^2\right)(g_{cl}^2 + (4\pi f c_{cl})^2)}} \quad \text{(A3.6)}$$

$$\varphi_f = atan2\left(-2\pi f c_{post} g_{cl} - 4\pi f c_{cl} g_{post}, -g_{post} g_{cl} + (2\pi f)^2 c_{post} c_{cl}\right) \quad \text{(A3.7)}$$

This can be further simplified by assuming that $g_{cl} \gg 4\pi f c_{cl}$ and $2\pi f c_{post} \gg g_{post}$:

$$\left|\frac{V_{post}}{V_{pre}}\right| = \frac{(2\pi f c_{cl})^2}{2\pi f c_{post} g_{cl}} = \frac{2\pi f {c_{cl}}^2}{c_{post} g_{cl}} = 2\pi f \tau_{cl} \frac{c_{cl}}{c_{post}} \quad \text{(A3.8)}$$

$$\varphi_f = atan2\left(-2\pi f c_{post} g_{cl}, -g_{post} g_{cl} + (2\pi f)^2 c_{post} c_{cl}\right)$$

$$= atan2\left(-2\pi f \tau_{post}, (2\pi f)^2 \tau_{cl} \tau_{post} - 1\right) \quad \text{(A3.9)}$$

Question A4: what is the impact of a current injected into the cleft on the VC prespike?

This Appendix deals with the question how i_{post} relates to i_{ion}, which is relevant for how the calcium current changes the prespike. The current i_{ion} that runs through the presynaptic cleft-facing membrane can leak away through the cleft leak conductance or via the postsynaptic cell. How these currents distribute depend on the relative admittances:

$$\frac{I_{post}}{I_{ion}} = \frac{-jY_5}{Y_3 + Y_{ion} - j(Y_2 + Y_5)} \quad \text{(A4.1)}$$

which becomes equation A1.1 when we assume that $g_{ion} << g_{cl}$ and $Y_2 = Y_5$.

We know that the calcium current during a presynaptic AP approaches a Gaussian function with a peak amplitude of 1.0-2.0 nA, a standard deviation τ_{Ca} of 0.21 ms and a calcium charge q_{Ca} of ~1 pC [44, 107]. The Gaussian function has the advantage that its Fourier transform is exact, allowing us to derive an exact solution for the impact of the calcium current on the postsynaptic prespike.

The Gaussian function to describe the calcium current over time is:

$$i_{ca} = \frac{q_{Ca}}{\tau_{Ca}\sqrt{2\pi}} e^{-\frac{t^2}{2\tau_{Ca}{}^2}} \quad or \;\; i_{max} e^{-\frac{t^2}{2\tau_{Ca}{}^2}} \qquad \text{(A4.2)}$$

Its Fourier transform is:

$$I_{Ca} = \int_{-\infty}^{\infty} i_{ca}\, e^{j2\pi f t} dt = \int_{-\infty}^{\infty} \frac{q_{Ca}}{\tau_{Ca}\sqrt{2\pi}} e^{-\frac{t^2}{2\tau_{Ca}{}^2}}\, e^{j2\pi f t} dt = \frac{q_{Ca}}{\tau_{Ca}\sqrt{2\pi}} \int_{-\infty}^{\infty} e^{\frac{-1}{2\tau_{Ca}{}^2}(t^2 - j4\pi\tau_{Ca}{}^2 f t)} dt$$

$$= \frac{q_{Ca}}{\tau_{Ca}\sqrt{2\pi}} \int_{-\infty}^{\infty} e^{\frac{-1}{2\tau_{Ca}{}^2}\left(t^2 - 2t\left(2\pi j\tau_{Ca}{}^2 f\right) + \left(2\pi j\tau_{Ca}{}^2 f\right)^2 - \left(2\pi j\tau_{Ca}{}^2 f\right)^2\right)} dt$$

$$= \frac{q_{Ca}}{\tau_{Ca}\sqrt{2\pi}} \int_{-\infty}^{\infty} e^{\frac{-1}{2\tau_{Ca}{}^2}\left(t - 2\pi j\tau_{Ca}{}^2 f\right)^2} dt \;\; e^{\frac{-1}{2\tau_{Ca}{}^2}\left(-2\pi j\tau_{Ca}{}^2 f\right)^2}$$

$$= \frac{q_{Ca}}{\tau_{Ca}\sqrt{2\pi}} \;\; \tau_{Ca}\sqrt{2\pi} \quad e^{-2(\pi\tau_{Ca} f)^2}$$

$$= q_{Ca}\, e^{-2(\pi\tau_{Ca} f)^2} \quad or \quad i_{max}\, \tau_{Ca}\sqrt{2\pi}\, e^{-2(\pi\tau_{Ca} f)^2} \qquad \text{(A4.3)}$$

To obtain the calcium current component of the prespike, we use equation A1.1 and assume that $g_{cl} >> 4\pi f c_{cl}$:

$$I_{post} = -j2\pi f \tau_{cl} I_{ca} = -j2\pi f \tau_{cl}\, q_{Ca}\, e^{-2(\pi\tau_{Ca} f)^2} \qquad \text{(A4.4)}$$

We perform the inverse Fourier transform by using that the Fourier transform of di_{Ca}/dt is equal to $j2\pi f I_{Ca}$:

$$i_{post} = \int_{-\infty}^{\infty} I_{post}\, e^{-j2\pi f t} df = \int_{-\infty}^{\infty} -j2\pi f \tau_{cl} I_{ca}\, e^{-j2\pi f t} df = -\tau_{cl} \int_{-\infty}^{\infty} j2\pi f I_{ca}\, e^{-j2\pi f t} df$$

$$= -\tau_{cl} \frac{di_{ca}}{dt} \qquad \text{(A4.5)}$$

$$-\tau_{cl}\frac{di_{ca}}{dt} = -\frac{\tau_{cl}q_{Ca}}{\tau_{Ca}{}^{3}\sqrt{2\pi}}\ t\ e^{-\frac{t^2}{2\tau_{Ca}{}^2}}\quad or\quad -\frac{\tau_{cl}i_{max}}{\tau_{Ca}{}^{2}}\ t\ e^{-\frac{t^2}{2\tau_{Ca}{}^2}} \qquad \text{(A4.6)}$$

This function will show two peaks at $t = \pm\tau$ with an amplitude of:

$$i_{post}(\pm\tau) = \pm\frac{\tau_{cl}}{\tau_{Ca}{}^{2}\sqrt{2\pi e}}\ q_{Ca} = \pm\frac{\tau_{cl}}{\tau_{Ca}\sqrt{e}}\ i_{Ca,max} \qquad \text{(A4.7)}$$

We thus define a simple scaling factor $\tau_{cl}\,(\tau_{Ca}\sqrt{e})^{-1}$ that relates amplitude of the presynaptic calcium current to the amplitude of the calcium prespike.

Appendix B. Geometry

Question B1: What is the voltage profile in the synaptic cleft for a simplified synapse?

We assume a radially-symmetrical synapse with radius *r* and cleft height *h*. The capacitive current that enters the synaptic cleft equals:

$$i_{cap} = c_m v'_{pre} = C_m \pi r^2 v'_{pre} \qquad \text{(B1.1)}$$

with v'_{pre} indicating the first temporal derivative of the presynaptic AP. We assume that the current is homogeneously distributed over the cleft-facing membrane and that all currents within the cleft run radially towards the interstitial fluid. The current density $k(x)$ (typically denoted J, but we use *k* instead to avoid confusion with our imaginary *j*) can be defined as a quasi-static function of the radial location *x*, where 0 indicates the center and *r* the synapse edge. $k(x)$ will be equal to the current that runs through the cleft-facing membrane from the center to radius x divided by the surface through which it escapes, $A_{esc}(x)$. This surface is the surface of an open cylinder with radius x and height *h*:

$$k(x) = \frac{i(x)}{A_{esc}(x)} = \frac{\pi x^2 C_m v'_{pre}}{2\pi x h} = \frac{C_m v'_{pre}}{2h}x \qquad \text{(B1.2)}$$

Based on $k(x)$, the electric field can be defined using a homogeneous extracellular cleft resistivity R_{ex}, where the negative sign reflects the convention that current runs down the voltage gradient:

$$-\frac{dv(x)}{dx} = R_{ex}k(x) = \frac{R_{ex}C_m v'_{pre}}{2h}x \qquad \text{(B1.3)}$$

The voltage profile relative to the cleft edge is the integral of equation B1.3 from x to r:

$$v(x) = \int_x^r \left(-\frac{R_{ex}C_m v'_{pre}}{2h}x\right)dx = -\frac{R_{ex}C_m v'_{pre}}{2h}\int_x^r (x)dx = \frac{R_{ex}C_m v'_{pre}}{4h}(r^2 - x^2) \qquad \text{(B1.4)}$$

We can also rewrite equation B1.4 as a relative distance to the cleft edge:

$$v(x/r) = \frac{r^2 R_{ex}C_m v'_{pre}}{4h}(1 - (x/r)^2) \qquad \text{(B1.5)}$$

The voltage profile will apply as long as all current runs radially to the extracellular matrix. When this is not the case -for instance, when currents enter into the postsynaptic cell or return through the presynaptic cleft-facing membrane- the current density will be reduced, and the voltage gradient will be reduced as well.

Question B2: How much current will be generated at the postsynaptic membrane?

We assume that the currents that run through the postsynaptic membrane are purely capacitive:

$$i_{post} = \int_{x=0}^r i_{cap}(x)dx = \int_{x=0}^r (C_m A(x)v'(x))dx \qquad \text{(B2.1)}$$

Here, the current through an annulus of membrane (at x, with thickness dx) will depend on the radial location as the surface of the annulus equals $2\pi x$dx and the cleft potential is also defined by the radial location (equation B1.4). Only v'_{pre} will be affected by the time derivative, which will become the second time derivative (v''_{pre}) . The equation then becomes:

$$i_{post} = C_m \int_{x=0}^r \left(2\pi x \frac{R_{ex}C_m v''_{pre}}{4h}(r^2 - x^2)\right)dx$$

$$= \frac{\pi R_{ex} C_m^2 v''_{pre}}{2h} \int_{x=0}^{r} (x\,(r^2 - x^2))dx$$

$$= \frac{\pi R_{ex} C_m^2 v''_{pre}}{2h} \left[\frac{1}{2} r^2 x^2 - \frac{1}{4} x^4\right]_{x=0}^{r}$$

$$= \frac{\pi R_{ex} C_m^2 v''_{pre}}{8h} r^4 \qquad \text{(B2.2)}$$

Question B3: How does the cleft resistivity relate to the cleft conductance?

With our phasor analysis we defined that (A2.6 after Fourier transformation):

$$i_{post} = \frac{(c_{cl})^2}{g_{cl}} v''_{pre} \qquad \text{(B3.1)}$$

By combining equation B2.2 and B3.1 we find that g_{cl} relates to the cleft resistivity:

$$g_{cl} = \frac{8\pi h}{R_{ex}} \qquad \text{(B3.2)}$$

Combining equations B3.1 and B3.2 yields an alternative way to calculate the extracellular resistivity:

$$R_{ex} = \frac{i_{post}\, 8\pi h}{c_{cl}^2\, v''_{pre}} \qquad \text{(B3.3)}$$

Question B4. What are the relations for a finger-like synapse?

We assume a sheet-like synapse with a cleft height *h*, a constant width of 2*r*, and a length *L* that is closed at the longitudinal ends. Any current that enters the synaptic cleft cannot escape along the longitudinal axis, leaving only the transversal route to the interstitial space. Examples of such synapses are finger-like synapses, such as the neuromuscular junction or the endbulb of Held synapse for which we ignore the longitudinal endings, or deeply-invaginating, cylindrical synapses (spinules) with a circular longitudinal

axis (*i.e.* a rolled-up sheet forming a cylinder). Because of the constant width, the voltage profile will be identical along the longitudinal axis, varying only along the synapse width. The capacitive current will be equal to $i_{cap}(x) = C_m v'_{pre} drdl$ (B4.1).

The current density *k* at each location will be:

$$k(x) = \frac{i(x)}{A_{esc}(x)} = \frac{C_m v'_{pre} xdl}{hdl} = \frac{C_m v'_{pre}}{h} x \qquad \text{(B4.2)}$$

The voltage gradient then is:

$$-\frac{dv(x)}{dx} = R_{ex} k(x) = \frac{R_{ex} C_m v'_{pre}}{h} x \qquad \text{(B4.3)}$$

And the voltage at x is:

$$v(x) = -\frac{R_{ex} C_m v'_{pre}}{h} \int_x^r (x) dx = \frac{R_{ex} C_m v'_{pre}}{2h} (r^2 - x^2) \qquad \text{(B4.4)}$$

The changes in the cleft potential will generate a postsynaptic, capacitive current. To calculate the total current from the finger-like synapse, we sum the current along the two dimensions:

$$i_{fin} = \int_{l=0}^{L} 2 \int_{x=0}^{r} i_{cap}(x) dx\, dl = \int_{l=0}^{L} 2 \int_{x=0}^{r} C_m A v'(x) dx\, dl$$

$$= \int_{l=0}^{L} 2 \int_{x=0}^{r} C_m \frac{R_{ex} C_m v''_{pre}}{2h} (r^2 - x^2) dx\, dl = \frac{R_{ex} C_m^2 v''_{pre}}{h} \int_{l=0}^{L} \int_{x=0}^{r} (r^2 - x^2) dx\, dl$$

$$= \frac{R_{ex} C_m^2 v''_{pre}}{h} \int_{l=0}^{L} \left[xr^2 - \frac{1}{3} x^3 \right]_{x=0}^{r} dl = \frac{2 R_{ex} C_m^2 v''_{pre} r^3}{3h} \int_{l=0}^{L} dl$$

$$= \frac{2 R_{ex} C_m^2 v''_{pre} r^3 L}{3h} \qquad \text{(B4.5)}$$

For the sheet-like synapse, x=0 indicates the cleft center and currents can run in two, transversal directions. We therefore multiply the capacitive current by 2 at the start of the derivation of B4.5. For a spinule synapse, no current can escape from the ‘deep’ end of the cylinder (at x=0) and therefore the

currents run in a single, transversal direction. The right-hand side of B4.5 should therefore be halved for spinule-like synapses or other deeply-invaginating synapses, neglecting any contribution from the cup-shaped cleft at the deep end. The characteristic difference between the radial-like or sheet-like synapse is whether the escape area along the longitudinal axis increases or stays constant, respectively. Following the logic outlined in B1, B2 and B4, one can calculate the cleft potentials and postsynaptic currents for other synaptic geometries.

Question B5. How does fenestration change the cleft potential and the VC prespike?

To assess the impact of fenestration on the cleft potential and the VC prespike, we compare a radially-symmetric synapse and a synapse with *n* equally-sized fingers. The relative cleft potential can be calculated using equation B1.5 for the radially-symmetric synapse (v_{sym}) and equation B4.4 for the finger-like synapse (v_{fin}), while assuming that the cleft potential of each finger is independent from each other:

$$\frac{v_{fin}}{v_{sym}} = \frac{{r_{fin}}^2 R_{ex} C_m v'_{pre}(1 - x^2/r_{fin}^2)}{2h} \frac{4h}{r_{sym}^2 R_{ex} C_m v'_{pre}(1 - x^2/r_{sym}^2)}$$

$$= \frac{2r_{fin}^2(1 - x^2/r_{fin}^2)}{r_{sym}^2(1 - x^2/r_{sym}^2)} \qquad \text{(B5.1)}$$

This gives at the center (x=0) a ratio of:

$$\frac{v_{fin}}{v_{sym}} = 2\left(r_{fin}/r_{sym}\right)^2 \qquad \text{(B5.2)}$$

To compare the VC prespike of a radially-symmetric synapse and a fenestrated synapse, we assume that the currents from each finger are synchronized and that they sum linearly. We use equation B2.2 and equation B4.5:

$$\frac{n\, i_{fin}}{i_{sym}} = \frac{2nR_{ex}C_m^2 {v''}_{pre} r_{fin}^3 L}{3h} \frac{8h}{\pi R_{ex} C_m^2 {v''}_{pre} r_{sym}^4} = \frac{16nLr_{fin}^3}{3\pi r_{sym}^4} \qquad \text{(B5.3)}$$

We assume that the total contact surface is conserved, so the surface of the fenestrated synapse ($n\ 2r_{fin}\ L$) and the radially-symmetric synapse (πr_{sym}^2) should be equal. Therefore $L = \pi r_{sym}^2 (n\ 2r_{fin})^{-1}$, which we insert into equation B5.3:

$$\frac{n\ i_{fin}}{i_{sym}} = \frac{16 n r_{fin}^3\ \pi r_{sym}^2}{3\pi r_{sym}^4\ \ n\ 2r_{fin}} = \frac{8}{3}\left(r_{fin}/r_{sym}\right)^2 \qquad \text{(B5.4)}$$